

# Functional Peaks-over-threshold Analysis

Raphaël de Fondeville \*

*Swiss Data Science Center, Lausanne, Switzerland*

and Anthony C. Davison †

*Chair of Statistics, École Polytechnique Fédérale de Lausanne, Lausanne, Switzerland*

## Abstract

Peaks-over-threshold analysis using the generalized Pareto distribution is widely applied in modelling tails of univariate random variables, but much information may be lost when complex extreme events are studied using univariate results. In this paper, we extend peaks-over-threshold analysis to extremes of functional data. Threshold exceedances defined using a functional  $r$  are modelled by the generalized  $r$ -Pareto process, a functional generalization of the generalized Pareto distribution that covers the three classical regimes for the decay of tail probabilities. This process is the only possible limit for the distribution of  $r$ -exceedances of a properly rescaled process. We give construction rules, simulation algorithms and inference procedures for generalized  $r$ -Pareto processes, discuss model validation, and use the new methodology to study extreme European windstorms and heavy spatial rainfall.

*Key words:* Functional regular variation; Peaks-over-threshold analysis; Rainfall;  $r$ -Pareto process; Spatial statistics; Statistics of extremes; Windstorm.

---

\*raphael.de-fondeville@epfl.ch

†anthony.davison@epfl.ch

# 1 Introduction

Extreme value theory provides a mathematical framework for the description and modelling of tails of statistical distributions that can be used to extrapolate beyond observed events. This theory has been studied extensively in a univariate framework (Fisher and Tippett, 1928; Gnedenko, 1943; Pickands, 1975) and is widely used in finance, insurance, telecommunications and the environmental sciences (Hosking and Wallis, 1987; Katz et al., 2002; Embrechts et al., 1997). However many complex phenomena are bowdlerised when modelled using the univariate theory, so richer approaches to modelling high-dimensional data have been explored over the past decade.

Max-stable processes (de Haan and Ferreira, 2006, Section 9.2) provide a functional extension of the classical extreme value distributions and have successfully been used to model maxima, but these models are difficult to fit in high dimensions (Huser and Davison, 2013). Moreover they involve a conflation of individual extremal events that discards information and can make it difficult to detect mixtures of tail behaviours. For example, in some regions rainfall events are either convective, and hence locally very intense, or cyclonic, with larger spatial accumulations of water but lower local intensities. Although driven by different weather patterns, both may lead to flooding, and, as suggested by Figure 1, the marginal distributions of their tails and their spatio-temporal structures may differ greatly. Even though large-scale events may also be damaging, reduction of the data to maxima tends to drive modelling to focus on small-scale but intense events that produce most maxima.

In the one-dimensional case the analysis of threshold exceedances is often preferred to that of block maxima. The approach originated in hydrological literature under the name of ‘peaks over threshold’ (POT) or ‘partial duration series’ analysis (Todorovic and Zelenhasic, 1970; Todorovic and Rousselle, 1971; NERC, 1975), its goal being to include all large individual events and thus provide more information than can be extracted from block, typically annual, maxima. This is particularly important when the data are limited and there is an appreciable seasonal component. A probabilistic basis for threshold modelling was provided by Balkema

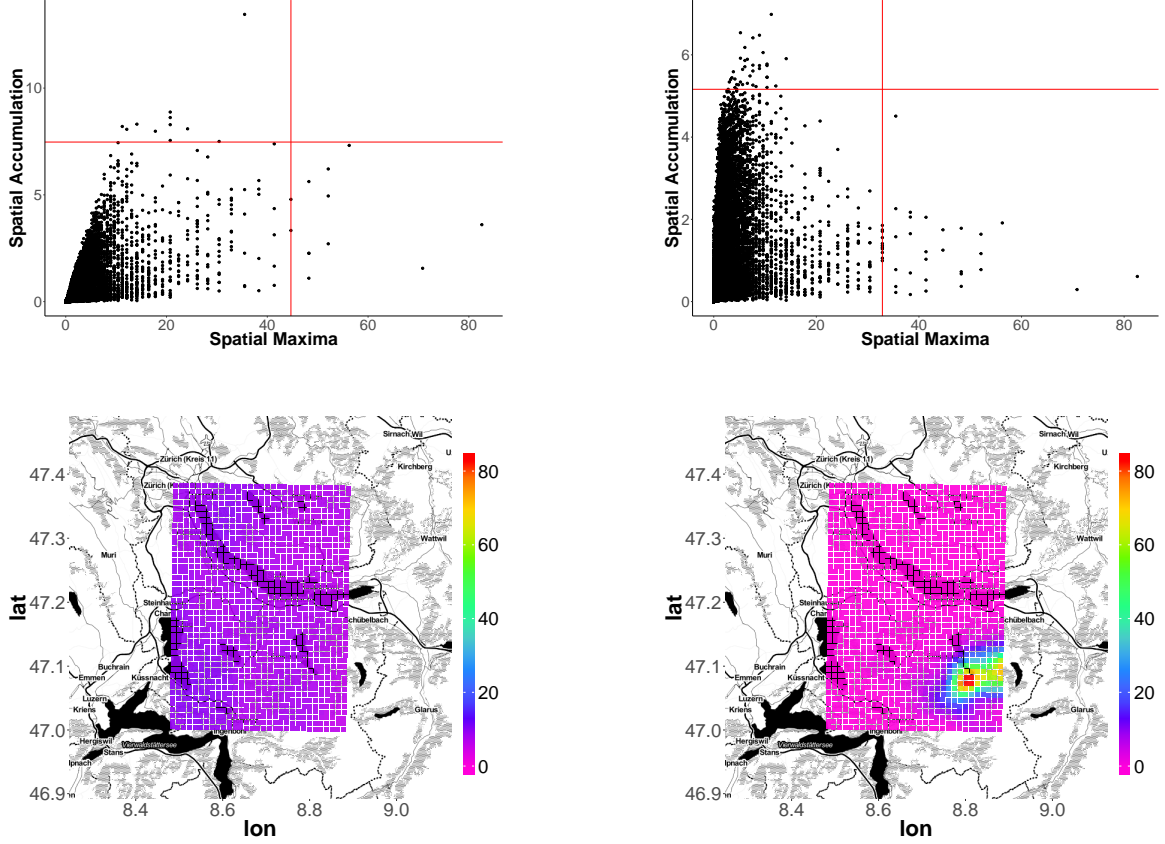


Figure 1: Extreme hourly rainfall events in the Zurich region, 2013–2018, computed using radar rainfall measurements  $X(s)$  (mm) on a grid  $S$ . Top left: spatial averages  $|S|^{-1} \int_S X(s) ds$  and spatial maxima  $\max_{s \in S} X(s)$ , with red thresholds demarcating the largest 11 events of each type. Top right: likewise for modified spatial averages and spatial maxima and thresholds for the largest 36 events of each type. Bottom line: events corresponding to the largest spatial average (left) and the largest spatial maximum (right).

and de Haan (1974) and Pickands (1975), and statistical aspects were developed by Davison (1984), Smith (1984) and Davison and Smith (1990). The basic idea is to fit the generalized Pareto distribution to the exceedances of a variable such as river flow or pollution level over a threshold, and a large subsequent literature has built on this early work and the method and its many variants have been applied in numerous other contexts.

In some applications it is helpful to reduce multivariate data to scalar structure variables (Coles and Tawn, 1994) that can be analysed using POT or other univariate methods, but this approach gives no insight into the combinations of variables yielding a rare event. Different structure variables may have different tail behaviours, moreover, possibly due to the presence of several underlying physical processes. Functional peaks-over-threshold analysis modifies this approach to give different perspectives on the dependence structure and provides a theoretical foundation for the detection of mixtures of tail behaviours through definitions of functional extremes tailored to particular types of events, as illustrated in Figure 1.

Existing functional peaks-over-threshold procedures rely on particular types of exceedances (Ferreira and de Haan, 2014) or are limited to settings where the data must have unbounded support and share the same polynomial-type tail decay (Dombry and Ribatet, 2015). Observations can be transformed to have a common marginal distribution, such as the unit Fréchet (Coles and Tawn, 1991, Section 5) or unit Pareto (Kluppelberg and Resnick, 2008), and exceedances defined on this transformed scale, but as many extreme phenomena are most naturally characterized on the scale of the original data, the use of transformations can require the user to make a compromise between interpretability and mathematical rectitude; see de Fondeville and Davison (2018) for attempts to characterize different types of rainfall after transformation of the data. In univariate extreme value theory, the generalized Pareto distribution provides a single framework for the modelling the original data in any of the classical Weibull, Gumbel or Fréchet regimes. This paper provides a similar unified formulation for functional peaks-over-threshold analysis under the assumption that the process has the same tail decay over its domain. This restriction on the tail behaviour is necessary to define

the exceedances directly on the original process, as otherwise the region or location with the heaviest tail dominates the limit distribution, leading to unrealistic models. We extend Dombry and Ribatet (2015) by introducing the generalized  $r$ -Pareto process, allowing more flexible definitions of rare events and generalized Pareto margins for tails. The generalized  $r$ -Pareto process is the only limit of exceedances of a properly rescaled regularly varying process. For some definitions of exceedances, it can be factorized to enable simulation of events with a fixed intensity, i.e., events for which the risk measure has a pre-determined return level.

Section 2 reviews classical univariate results and introduces functional peaks-over-threshold analysis. We derive convergence results for the three tail decay regimes and we define and characterize the generalized  $r$ -Pareto process, emphasising its relation with max-stable processes and presenting simulation algorithms. Section 3 introduces a general model for functional exceedances. In Section 4, we discuss statistical inference and in Section 5 describe methods for model validation. In Section 6 we use our ideas to develop a stochastic weather generator for windstorms over Europe, and Section 7 illustrates the importance of risk definition when studying potential flooding in the city of Zurich. Technical details and proofs of the main results are relegated to Appendices.

## 2 Modelling exceedances over a high threshold

### 2.1 Univariate model

If  $X$  is a random variable with distribution function  $F$  for which there exist sequences of constants  $a_n > 0$  and  $b_n$  such that

$$n \Pr \left( \frac{X - b_n}{a_n} > x \right) \rightarrow -\log G(x), \quad n \rightarrow \infty, \quad (1)$$

where  $G$  is a non-degenerate distribution function, then  $X$  is said to belong to the max-domain of attraction of  $G$  (Resnick, 1987, p. 12). For a large enough threshold  $u < \inf\{x : F(x) = 1\}$ , its tail distribution can be approximated by a generalized Pareto distribution,

$$\Pr(X - u > x \mid X > u) \approx H_{(\xi, \sigma)}(x) = \begin{cases} (1 + \xi x/\sigma)_+^{-1/\xi}, & \xi \neq 0, \\ \exp(-x/\sigma), & \xi = 0, \end{cases} \quad (2)$$

where  $\sigma = \sigma(u) > 0$  and, here and below,  $a_+ = \max(a, 0)$  for real  $a$ . The shape parameter  $\xi$  is also called the tail index. If  $\xi$  is negative then  $x$  must lie in the interval  $[0, -\sigma/\xi]$ , whereas if  $\xi \geq 0$  then  $x$  can take any positive value. The random variable  $X$  is said to belong to the Weibull, Gumbel or Fréchet domains of attraction if  $\xi$  is respectively negative, zero or positive. The max-domain of attraction conditions are satisfied by many random variables (e.g., Beirlant et al., 2004, pp. 59, 62, 72). Davison and Smith (1990) use equation (2) as the basis of the approximation

$$F(x) \approx 1 - \zeta_u H_{(\xi, \sigma)}(x - u), \quad x > u, \quad (3)$$

where  $\zeta_u$  denotes the probability that  $X$  exceeds the threshold  $u$ . This offers a general, flexible and unified model for distribution tails and is widely used to estimate probabilities of rare events.

In its simplest form equation (3) applies to independent and identically distributed variables, but it may also be applied to dependent, non-stationary and spatial data. The modelling of exceedances has been extended to multivariate settings (Rootzén and Tajvidi, 2006; Rootzén et al., 2018b,a) and to continuous processes (Ferreira and de Haan, 2014; Dombry and Ribatet, 2015).

## 2.2 Functional exceedances

Let  $S \subset \mathbb{R}^D$  ( $D \geq 1$ ) be a compact metric space, let  $\mathcal{F}$  denote the Banach space of real-valued continuous functions on  $S$  with norm  $\|\cdot\|$ , and let  $\mathcal{F}_+$  denote the subset of  $\mathcal{F}$  containing only non-negative functions that are not everywhere zero; thus  $\mathcal{F}_+$  excludes the zero function, thereby avoiding the appearance of degenerate limiting probability measures.

It is straightforward to define the exceedance of a scalar random variable  $X$  over a threshold  $u$ . An appropriate approach for random functions is through risk functionals and  $r$ -exceedances. A risk functional  $r$  is defined to be a continuous mapping from  $\mathcal{F}$  into  $[0, \infty)$  and an  $r$ -exceedance is an event of the form  $\{r(X) \geq u\}$  for some  $u \geq 0$ , i.e., an event for which the scalar  $r(X)$  exceeds a threshold  $u$ . This definition was introduced by Dombry and Ribatet (2015) for homogeneous ‘cost functionals’ on  $\mathcal{F}_+$ , i.e., functionals for which there exists  $\kappa > 0$  such that  $r(ay) = a^\kappa r(y)$  when  $y \in \mathcal{F}_+$  and  $a > 0$ . The term ‘radial aggregation function’ has also been used (Opitz, 2013b), but we prefer to use ‘risk functional’, which we think better reflects how  $r(X)$  measures the severity of  $X$  in terms of the risk summarised by  $r$ .

Functional threshold exceedances were studied using  $r(X) = \sup_{s \in S} X(s)$  by Ferreira and de Haan (2014) for continuous processes, but this functional treats as extreme all events with an exceedance at at least one location and requires that  $x(s)$  is observed throughout  $S$ . Coles and Tawn (1996) had earlier modelled areal rainfall via large values of  $\int_S X(s) ds$ , and other risk functionals such as  $\int_S X^2(s) ds$  for a proxy of the energy inside a climatic system (Powell and Reinhold, 2007),  $\min_{s \in S'} X(s)/u(s)$  for exceedances over dams,  $X(s_0)$  for risks impacting a specific location  $s_0$ , and so forth, may arise in applications. The motivation behind the present paper is to define risk functionals tailored to specific types of physical processes, naturally yielding different models for different functionals. When motivated by engineering or other considerations, it might be desirable to have a unique model for different notions of risk, and if so, consistency between definitions can be enforced in our framework

by studying

$$r(X) = \max \{r_1(X) - u_1, \dots, r_M(X) - u_M\},$$

where  $r_1, \dots, r_M$  are the functionals of interest and  $u_1, \dots, u_M$  the corresponding thresholds.

In this work we generalize  $r$ -exceedances under minimal assumptions on the risk functional and derive limit distributions for the three tail decay regimes. Convergence results are more easily presented for linear risk functionals, so we focus on them in the main paper, relegating details and more general results to the Appendices. Thus for now we consider functionals for which  $r(x + y) = r(x) + r(y)$  for any  $x, y \in \mathcal{F}$ .

## 2.3 Functional $r$ -exceedances

### 2.3.1 Notation, assumptions and convergence

Let  $\xi$  be a real-valued shape parameter,  $a \equiv a(s)$  a continuous positive function and  $b \equiv b(s)$  a continuous function, both defined for  $s \in S$ . Let  $\mathcal{F}_0 = \mathcal{F}_+ \cup \{0\}$ , and define the sets

$$\mathcal{F}^{\xi, a, b} = \begin{cases} \mathcal{F}_+ - \{b - \xi^{-1}a\}, & \xi > 0, \\ \mathcal{F}, & \xi = 0, \\ \{b - \xi^{-1}a\} - \mathcal{F}_+, & \xi < 0, \end{cases}$$

i.e., the positive quadrant in  $\mathcal{F}$ , shifted by  $b - a/\xi$ , and also reflected when  $\xi < 0$ . For future use and with a given risk functional  $r$  on  $\mathcal{F}$  we also define

$$\mathcal{S}_r^{\xi, a} = \begin{cases} \{y \in \mathcal{F}_+ : r(ay^\xi) \geq 1, \|y\| = 1\}, & \xi \neq 0, \\ \{y \in \mathcal{F}_+ : r(a \log y) = 0\}, & \xi = 0. \end{cases}$$

Given functions  $a$  and  $b$  and threshold  $u \geq 0$ , a risk functional can take values only in the intervals  $\mathcal{U}_r^\xi(u) = [u, \infty)$  if  $\xi \geq 0$  and  $\mathcal{U}_r^\xi(u) = [u, r(b) - \xi^{-1}r(a))$  if  $\xi < 0$ .

In this section,  $X$  denotes a stochastic process with sample paths in  $\mathcal{F}$  for which there exist a real number  $\xi$ , sequences  $\{a_n\}_{n=1}^\infty > 0$  and  $\{b_n\}_{n=1}^\infty$  of continuous functions on  $S$ , and



a suitable measure  $\Lambda$  on  $\mathcal{F}_+$  such that

$$\left. \begin{aligned} n \Pr \left[ \left\{ 1 + \xi \left( \frac{X - b_n}{a_n} \right) \right\}_+^{1/\xi} \in \cdot \right], \quad \xi \neq 0 \\ n \Pr \left\{ \exp \left( \frac{X - b_n}{a_n} \right) \in \cdot \right\}, \quad \xi = 0 \end{aligned} \right\} \rightarrow \Lambda(\cdot), \quad n \rightarrow \infty, \quad (4)$$

where  $\{a(s)\}_+ = \max\{a(s), 0\}$  is a function of  $s$  and  $a_n$  and  $b_n$  are chosen such that for any  $s \in S$ ,

$$\lim_{n \rightarrow \infty} n \Pr \left\{ \frac{X(s) - b_n(s)}{a_n(s)} > x \right\} = \begin{cases} (1 + \xi x)_+^{-1/\xi}, & 1 + \xi x > 0, \xi \neq 0, \\ \exp(-x), & x > 0, \xi = 0. \end{cases} \quad (5)$$

Equation (4) involves a specific type of convergence described in the Appendices and defines a general form of functional regular variation (Hult and Lindskog, 2005) introduced by Ferreira and de Haan (2014); we write  $X \in \text{GRV}(\xi, a_n, b_n, \Lambda)$ . General functional regular variation is the natural functional extension of (1): any model of dependence using approximation (3) should be linked to some form of general functional regular variation.

The main limitation of our assumptions is not the existence of a limiting measure in (4), but rather the restriction of  $\Lambda$  to the space of continuous functions, which does not allow any type of asymptotic independence (Ledford and Tawn, 1996). Studying more general spaces, such as continuous functions for which the set of discontinuities has zero measure, is left for future work. A second restriction in (4) is that  $\xi$  is constant over  $S$ : since we compute the risk directly using  $X$ , useful convergence results are obtained only if the shape parameter is constant—if  $\xi$  varies over  $S$  then either those locations with the highest values of  $\xi$  or those with the highest upper bound determine the asymptotic tail behaviour and then the limiting dependence cannot be modelled. For environmental applications, the unique  $\xi$  should be considered to drive the tail regime of the physical process that is characterised by the functional  $r$ , for instance convective rainfall. As mentioned above, this restriction can be relaxed by transforming data to have the same rate of tail decay throughout  $S$ , though

typically at the cost of losing the physical interpretation of the exceedances.

The limiting measure  $\Lambda$  in (4) is homogeneous of order  $-1$  (Lindskog et al., 2014, Theorem 3.1), i.e.,  $\Lambda(t\mathcal{A}) = t^{-1}\Lambda(\mathcal{A})$  for any positive scalar  $t > 0$  and Borel set  $\mathcal{A} \subset \mathcal{F}_+$ . This property allows extrapolation from observed to unobserved extreme events.

We also suppose that the sequence of functions  $a_n$  satisfies

$$\lim_{n \rightarrow \infty} \sup_{s \in S} \left| \frac{a_n(s)}{r(a_n)} - A(s) \right| = 0, \quad (6)$$

so we can write  $a_n(s) \approx r(a_n)A(s)$  for large  $n$ . A similar assumption was used in Ferreira et al. (2012) and Engelke et al. (2019) and seems reasonable in many environmental applications. For instance, assuming that the marginal distributions belong to a location-scale family  $F[\{x(s) - B(s)\}/A(s)]$  that describes the behaviour of the underlying physical process characterized by the risk functional  $r$  implies both a common limiting shape parameter  $\xi$  and that we can choose  $a_n(s) = a'_n A(s)$  and  $b_n(s) = b'_n A(s) + B(s)$  with real-valued sequences  $a'_n > 0$  and  $b'_n$ .

Our first main result is the following.

**THEOREM 1.** *Let  $X$  be a stochastic process with sample paths in  $\mathcal{F}$  and let  $r$  be a linear risk functional if  $\xi \neq 0$  and an evaluation functional if  $\xi = 0$ , i.e.,  $r(x) = x(s)$  for some  $s \in S$ . If  $X \in \text{GRV}(\xi, a_n, b_n, \Lambda)$  and the functions  $a_n(s)$  satisfy (6), then*

$$\Pr \left\{ \left\lfloor \frac{X - b_n}{r(a_n)} \right\rfloor \in (\cdot) \mid r(X) \geq u_n \right\} \rightarrow \Pr \{P \in (\cdot)\}, \quad n \rightarrow \infty, \quad (7)$$

where  $u_n = r(a_n)u + r(b_n)$ ,  $u \in \mathcal{U}_r^\xi(0)$ , and  $P$  denotes a generalized  $r$ -Pareto process with tail index  $\xi$ , scale function  $A$ , zero location and measure  $\Lambda$ . When  $\xi > 0$ , we define  $\lfloor \cdot \rfloor = \max\{(\cdot), -\xi A\}$  with the maxima taken pointwise and  $\lfloor \cdot \rfloor = (\cdot)$  when  $\xi \leq 0$ .

In other words, generalized  $r$ -Pareto processes appear as limits for any stochastic process  $X$  that is regularly varying in the sense of (4), conditional on increasingly large  $r$ -exceedances.

When  $\xi = 0$ , the restriction to evaluation functionals is needed to obtain representations such as (8) below, but convergence for more general functionals is described in Appendix A.

### 2.3.2 Generalized $r$ -Pareto process: Definition and properties

We now describe generalized  $r$ -Pareto processes, give their properties, describe simulation algorithms and link them to max-stable processes.

DEFINITION 1. *Let  $\xi$  be a tail index, let  $a(s) > 0$  and  $b(s)$  be continuous functions on  $S$ , let  $r : \mathcal{F}^{\xi,a,b} \rightarrow \mathcal{U}_r^\xi$  be a linear risk functional, let  $\Lambda$  be a  $(-1)$ -homogeneous measure on  $\mathcal{F}_+$  and let  $A = a/r(a)$ . When  $\xi = 0$ , we also suppose that  $r$  is an evaluation functional. The generalized  $r$ -Pareto process  $P$  associated to the measure  $\Lambda$  and tail index  $\xi$  is the stochastic process on  $\{x \in \mathcal{F}^{\xi,a,b} : r(x) \geq r(b)\}$  defined by*

$$P = \begin{cases} \frac{r(a)}{\xi} R^\xi \frac{W_{\xi,A}}{r(W_{\xi,A})} + b - \xi^{-1}a, & \xi \neq 0, \\ r(a) \log(RW_{0,A}) + b, & \xi = 0, \end{cases} \quad (8)$$

where  $R$  is a scalar unit Pareto random variable independent of  $W_{\xi,A}$ , a stochastic process with state space  $S$  that takes values in  $\mathcal{S}_r^{\xi,A}$  and has probability measure

$$\sigma_r(\cdot) = \begin{cases} \frac{\Lambda \{y \in \mathcal{F}_+ : r(Ay^\xi) \geq 1, Ay^\xi / \|Ay^\xi\| \in (\cdot)\}}{\Lambda \{y \in \mathcal{F}_+ : r(Ay^\xi) \geq 1\}}, & \xi \neq 0, \\ \frac{\Lambda \{y \in \mathcal{F}_+ : r(y \exp A) \geq 1, A \log y - r(A \log y) \in (\cdot)\}}{\Lambda \{y \in \mathcal{F}_+ : r(y \exp A) \geq 1\}}, & \xi = 0. \end{cases} \quad (9)$$

This construction relies on a pseudo-polar decomposition: the process is the product of a radial component, namely a univariate Pareto variable representing the intensity of the process, and an angular component that determines how the process varies over  $S$ .

Generalized  $r$ -Pareto processes are closely related to the class of stochastic processes  $Y_r$  defined on

$$\mathcal{A}_r = \begin{cases} \{y \in \mathcal{F}_+ : r(Ay^\xi) \geq 1\}, & \xi \neq 0, \\ \{y \in \mathcal{F}_+ : r(A \log y) \geq 1\}, & \xi = 0, \end{cases} \quad (10)$$

with probability measure  $\Lambda(\cdot)/\Lambda(\mathcal{A}^r)$ , where  $\Lambda$  is a  $(-1)$ -homogenous measure on  $\mathcal{F}_+$ . A standard approach to modelling dependence in multivariate statistics relies on copulas, and requires that all the components of a random vector follow a uniform distribution. Similarly, in extreme-value modelling the marginal behaviour and dependence structure are typically handled separately, with the margins standardized to a common distribution such as the unit Pareto. We use  $Y_r$ , whose marginals are in the Fréchet domain of attraction with tail index  $\xi = 1$ , as the process of reference. Following (9), the angular process  $W_{\xi,A}$  can be constructed as

$$W_{\xi,A} = \begin{cases} \frac{AY_r^\xi}{\|AY_r^\xi\|}, & \xi \neq 0, \\ \exp\{A \log Y_r - r(A \log Y_r)\}, & \xi = 0, \end{cases} \quad (11)$$

and this is key to simulation of generalized  $r$ -Pareto processes. Following Dombry and Ribatet (2015) and de Fondeville and Davison (2018), there is a pseudo-polar decomposition

$$Y_r = R \frac{W_1}{r(W_1)}, \quad (12)$$

where  $R$  and  $W_1$  are independent,  $R$  is a unit Pareto random variable and  $W_1$  is a stochastic process with state space  $S$  and taking values in  $\mathcal{S} = \{y \in \mathcal{F}_+ : \|y\|_1 = 1\}$  with probability measure

$$\sigma_0(\cdot) = \frac{\Lambda\{y \in \mathcal{F}_+ : r(Ay^\xi) \geq 1, y/\|y\|_1 \in (\cdot)\}}{\Lambda\{y \in \mathcal{F}_+ : r(Ay^\xi) \geq 1, y/\|y\|_1 \in \mathcal{S}\}}, \quad (13)$$

where  $\|\cdot\|_1$  denotes the 1-norm on  $\mathcal{F}_+$ . The decomposition (12) is convenient because simulation of  $W_1$  at large finite number of locations is feasible for many common models (Thibaud and Opitz, 2015; Dombry et al., 2016).

One desirable and useful feature of generalized  $r$ -Pareto processes is that their marginal distributions are generalized Pareto. Consider a location  $s_0 \in S$  and a threshold  $u_0 \geq 0$  sufficiently high that the set  $\{x \in \mathcal{F}^{\xi,a,b} : x(s_0) > u_0\}$  lies within the set  $\{x \in \mathcal{F}^{\xi,a,b} : r(x) \geq r(b)\}$ .

Then the distribution of  $P(s_0)$  above the threshold  $u_0$  is of the generalized Pareto form

$$\Pr \{P(s_0) > x \mid P(s_0) > u_0\} = \left\{ 1 + \xi \frac{x - u_0}{\sigma(s_0)} \right\}^{-1/\xi}, \quad x \geq u_0, \quad (14)$$

where  $\sigma(s_0) = r(a)A(s_0) + \xi\{u_0 - b(s_0)\}$ .

The distribution of the risk  $r(P) - r(b)$  above  $r' \in \mathcal{U}^\xi(0)$  is also generalized Pareto, with shape and scale parameters  $\xi$  and  $r(a)$ . However, the process  $P$  itself is not threshold-stable in general, though its translation  $P + \xi^{-1}a - b$  is threshold-stable: if  $u \geq r(b)$ , then

$$\Pr \{P + \xi^{-1}a - b \in (\cdot) \mid r(P) \geq u\} = \Pr \left[ \frac{r(a) + \xi\{u - r(b)\}}{r(a)} (P + \xi^{-1}a - b) \in (\cdot) \right].$$

### 2.3.3 Simulation

The process  $Y_r$  defined through the pseudo-polar decomposition (12) is key to the construction of generalized  $r$ -Pareto processes and to their simulation. Simple algorithms to draw samples from  $Y_r$  exist for risk functionals such as  $r_1(x) = \|x\|_1$  or  $r_2(x) = \sup_{s \in S} x(s)$ ; see Asadi et al. (2015), for example. If a simulation algorithm for  $Y_r$  with risk functional  $r(X)$  is available, then we can sample from the angular component  $W_{\xi,A}$  using (11). We generalize the principle of de Fondeville and Davison (2018, Section 2.3) to develop an accept-reject algorithm for the generalized  $r$ -Pareto process when  $\xi \neq 0$ ; modification for  $\xi = 0$  is straightforward. If we can find a threshold  $u > 0$  such that

$$\{y \in \mathcal{F}_+ : r(Ay^\xi) \geq 1\} \subset \{y \in \mathcal{F}_+ : \|y\|_1 \geq u\},$$

then Algorithm 1 enables the simulation of a generalized  $r$ -Pareto process. It is particularly convenient, as it allows the simulation of events for a given value of the risk functional by replacing  $R_2$  by a return level of a unit Pareto variable. In the algorithm, every unit Pareto variable is independent of every other, and all have distribution function  $1 - 1/r$  for  $r > 1$ .

---

**Algorithm 1:** Simulation of generalized  $r$ -Pareto process,  $P$ 

---

Set  $Y_r = 0$ ;  
**while**  $r(AY_r^\xi) < 1$  **do**  
    generate a unit Pareto random variable  $R_1$ ;  
    generate  $W_1$  with probability measure  $\sigma_0$  given in (13);  
    set  $Y_r = R_1 W_1 / u$ ;  
**end**  
set  $W_2 = AY_r^\xi / \|AY_r^\xi\|$ . Generate a unit Pareto random variable  $R_2$ ;  
return  $P = r(a)\xi^{-1}R_2^\xi W_2 / r(W_2) + b - \xi^{-1}a$ .

---

### 2.3.4 Link to max-stable processes

In univariate extreme-value theory the marginal assumptions of equation (5) are equivalent to convergence of rescaled block maxima toward the generalized extreme value (GEV) distribution, i.e., for each  $s \in S$  we have

$$\lim_{n \rightarrow \infty} \Pr \left\{ \frac{\max_{j=1, \dots, n} X_j(s) - b_n(s)}{a_n(s)} \leq z \right\} = \begin{cases} \exp \left\{ - (1 + \xi z)_+^{-1/\xi} \right\}, & \xi \neq 0, \\ \exp \{ - \exp(-z) \}, & \xi = 0. \end{cases}$$

There is a similar relation between generalized  $r$ -Pareto processes and the functional extensions of GEV variables known as max-stable processes. The representation of these processes is not unique, and we use that of de Haan (1984), which relies on Poisson point processes. Consider  $(R_j, W_j)_{j=1, \dots, \infty}$  on  $(0, \infty) \times \mathcal{S}_r^{\xi, A}$  with intensity measure  $r^{-2} dr \times \sigma_r(dw)$ , where  $\sigma_r$  is given in Definition 1. Then the process

$$M(s) = \begin{cases} \sup_{j \geq 1} \frac{r(a)}{\xi} R_j^\xi \frac{W_j}{r(W_j)} + b(s) - \xi^{-1}a, & \xi \neq 0, \\ \sup_{j \geq 1} r(a) \log(R_j W_j) + b(s), & \xi = 0, \end{cases} \quad s \in S, \quad (15)$$

is max-stable with exponent measure  $\Lambda \circ T_{\xi, a, b}(\cdot)$  (Resnick, 1987, Proposition 3.7), where

$$T_{\xi, a, b}(z) = \begin{cases} \{1 + \xi(z - b)/a\}_+^{1/\xi}, & \xi \neq 0, \\ \exp \{ (z - b)/a \}, & \xi = 0. \end{cases}$$

The finite-dimensional distribution function of  $M(s)$  at locations  $s_1, \dots, s_L \in S$  is

$$\Pr \{M(s_l) < z_l, l = 1, \dots, L\} = \exp \left\{ -\Lambda \circ T_{\xi, a(s_l), b(s_l)} (\mathcal{A}_z) \right\}, \quad (16)$$

where  $\mathcal{A}_z$  is the complement in  $\mathbb{R}_+^L$  of the Cartesian product  $\times_{l=1}^L (0, z_l]$ . The exponent in expression (16) contains the measure of a generalized  $r$ -Pareto process with risk functional  $r(x) = \max_{l=1, \dots, L} x(s_l)$ ; see Appendix A for the definition of generalized  $r$ -Pareto process with non-linear risk functional. According to representation (15) the max-stable process  $M(s)$  is constructed using infinitely many single events of a Poisson process, and the  $r$ -exceedances of these events above a threshold  $u$  correspond to a generalized  $r$ -Pareto process; the latter also arises as the limit of  $r$ -exceedances for its corresponding max-stable process. The Poisson intensity, which is necessary to model the occurrence of single events in the max-stable process, becomes a Pareto distribution through conditioning on the  $r$ -exceedance. Outside the max-stable framework the number of exceedances need not be Poisson; for instance, seasonality or trend can be incorporated, as in Section 6.3.

### 3 Functional peaks-over-threshold modelling

We now describe a general approach to modelling  $r$ -exceedances of  $X$  over a high threshold. Theorem 2 suggests that in principle the choice of risk functional should not impact the model parameters, but in practice it affects what events are considered extreme, especially in the presence of a mixture in the tail behaviour, as illustrated by Figure 1. The choice of risk functional allows the user to focus on one component of a possible mixture by incorporating field-specific expertise, while improving sub-asymptotic behaviour by fitting the model using only those observations closest to the chosen type of extreme event.

Suppose we have a linear risk functional  $r$  whose exceedances occur for a single physical process, such as cyclonic rainfall, and that for such events it is reasonable to consider a tail index  $\xi$  constant over space. More specifically, suppose the marginal distributions of  $X(s)$

belong to a location-scale family with continuous positive scale function  $A(s)$ , continuous real location function  $B(s)$ , and distribution function  $F$  satisfying equation (1) with sequences  $a'_n > 0$  and  $b'_n$ . If so, the normalizing functions  $a_n(s)$  and  $b_n(s)$  for  $X(s)$  satisfy

$$a_n(s) = A(s)a'_n, \quad b_n(s) = B(s) + A(s)b'_n, \quad s \in S,$$

yielding the asymptotic decomposition implied by (6).

We impose a parametric structure on the extremal dependence of  $X$  and on the marginal scale and location functions  $A$  and  $B$ . The latter are assumed to belong to parametric families of functions  $\{A_{\theta_A} : \theta_A \in \Theta_A\}$  and  $\{B_{\theta_B} : \theta_B \in \Theta_B\}$ , where  $\Theta_A$  and  $\Theta_B$  are subsets of  $\mathbb{R}^{d_A}$  and  $\mathbb{R}^{d_B}$ , while the limiting measure  $\Lambda$  is supposed to be parametrised by  $\theta_\Lambda \in \Theta_\Lambda$ , which is a subset of  $\mathbb{R}^{d_\Lambda}$ .

To model the asymptotic dependence of  $X$  we suppose that  $X \in \text{GRV}(\xi, a_n, b_n, \Lambda)$ . The dependence properties of the limiting generalized  $r$ -Pareto process are determined by the angular process  $W_{\xi, A}$ , which must live on the unit sphere. To characterize and compare angular process models, we need a measure of dependence, but classical measures such as the covariance function or the semi-variogram

$$\gamma(h) = \frac{1}{2} \text{var}\{X(s') - X(s)\}$$

rely on the existence of moments and are typically undefined in our setting. A more suitable dependence measure is (de Fondeville and Davison, 2018)

$$\pi(s', s) = \lim_{q \rightarrow 1} \Pr[X(s') > u_q(s') \mid \{X(s) > u_q(s)\} \cap \{r(X) \geq u\}], \quad u \geq 0, \quad s, s' \in S, \quad (17)$$

where  $u_q(s)$  denotes the  $q$  quantile of  $X(s)$ . Equation (17) extends the extremogram (Davis and Mikosch, 2009) to  $r$ -exceedances and generalizes the extremal dependence coefficient  $\chi$  (Ledford and Tawn, 1996) to processes: it summarizes the pairwise extremal dependence



between  $X(s)$  and  $X(s')$ . Other measures of dependence exist (Smith, 1990; Cooley et al., 2006), but we prefer  $\pi$  for its interpretability.

Several models for  $W_{\xi,A}$  stem from the literature on max-stable processes. The Gaussian extreme value process, which relies on deterministic Gaussian kernels randomly shifted in space (Smith, 1990), is attractive for its computational tractability and relative simplicity, but it yields unrealistic random fields. Under the Brown–Resnick (1977), the angular process  $W_{\xi,A}$  is a log-Gaussian random function whose underlying Gaussian process has stationary increments, semi-variogram  $\gamma$  and mean equal to half of its variance. In this case, (17) reduces to

$$2 \left( 1 - \Phi \left[ \{ \gamma(h)/2 \}^{1/2} \right] \right),$$

where  $h = s - s'$  and  $\Phi$  denotes the standard normal cumulative distribution function. The Brown–Resnick model is particularly attractive because many semi-variogram functions available in the spatial statistics literature can be used to formulate models for extremal dependence. The behaviour of  $\gamma$  near the origins determines the smoothness of the generalized  $r$ -Pareto process and its behaviour as  $h \rightarrow \infty$  determines the extremal dependence regime. Indeed, if the semi-variogram is bounded, as is the case for strictly stationary Gaussian processes, then  $\pi(h) > 0$  for any  $h > 0$ , whereas if  $\gamma$  is unbounded then we obtain near-independence,  $\pi(h) \rightarrow 0$ , for large  $h$ ; see Figure 2. Choosing a log-Gaussian  $W_{\xi,A}$  implies that for any linear  $r$ ,  $\Lambda(\partial\mathcal{A}_r) = 0$ , where  $\partial\mathcal{A}_r$  is the boundary of the set  $\mathcal{A}_r$  defined in (10).

An alternative model, for which  $\Lambda(\partial\mathcal{A}_r) \neq 0$ , is the extremal- $t$  process (Opitz, 2013a)

$$W(s) \propto \max\{G(s), 0\}^\nu, \quad s \in S, \nu > 0,$$

where  $G$  is a strictly stationary Gaussian process with covariance function  $C$ . Enforcing the non-negativity of the underlying Gaussian process induces non-zero weights on the boundary of  $\mathcal{F}^{\xi,a,b}$ , making this a natural model for phenomena such as rainfall, but the model becomes

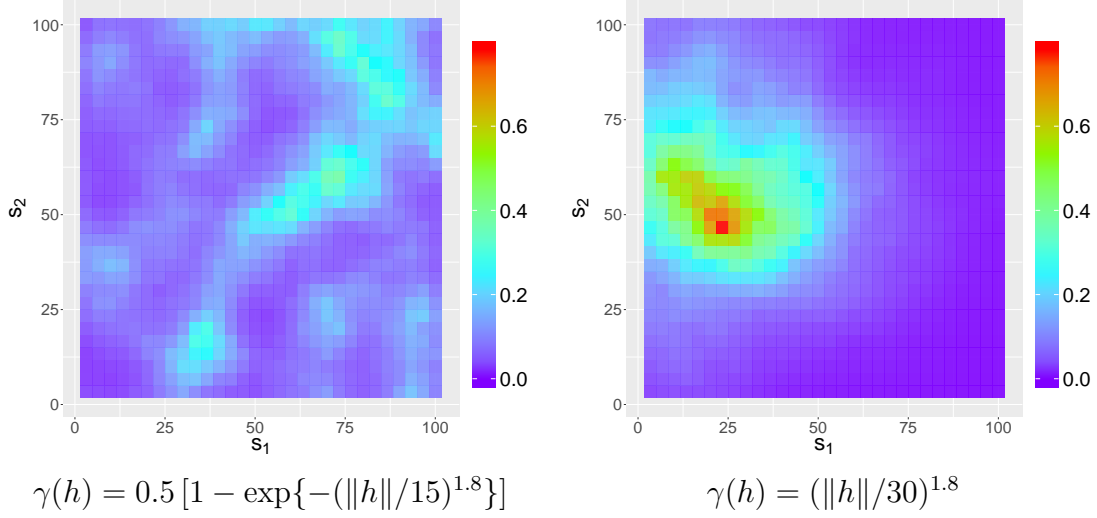


Figure 2: Simulated generalized  $r$ -Pareto processes with  $r(X) = \int_S X(s)ds = 100$  for two semi-variogram functions. Left: bounded power-exponential semi-variogram function. Right: unbounded power variogram.

improper when  $\xi < 0$ , as then  $\Pr\{X(s) = -\infty\} > 0$ . Its extremogram,

$$2 \left( 1 - t_{\nu+1} \left[ (\nu + 1)^{1/2} \left\{ \frac{1 - C(h)}{1 + C(h)} \right\}^{1/2} \right] \right),$$

must be at least  $2 [1 - t_{\nu+1} \{(\nu + 1)^{1/2}\}]$ , so the model can only reproduce strong dependence when  $\nu$  is low. This limitation weakens as  $\nu$  increases; then the model approaches the Brown–Resnick model, which is usually preferred for this reason.

In the next section we describe an approach to joint inference on the complete parameter vector

$$\theta = \{a'_n, b'_n, \theta_A, \theta_B, \theta_W\} \in (0, \infty) \times \mathbb{R} \times \Theta_A \times \Theta_B \times \Theta_W. \quad (18)$$

Identifiability issues may arise with the parametric models for  $A$  and  $B$ , which must be designed to ensure that  $r(A) = 1$  and, for instance,  $r(B) = 0$ .

## 4 Statistical inference

Statistical inference for  $r$ -exceedances of a stochastic process  $X \in \text{GRV}(\xi, a_n, b_n, \Lambda)$  is based on the approximation

$$\begin{aligned} \Pr(X \in \mathcal{A}) &= \Pr\{r(X) \geq u_n\} \times \Pr\{X \in \mathcal{A} \mid r(X) \geq u_n\}, \\ &\approx \Pr[1\{r(X) \geq u_n\} = 1] \times \Pr(P \in \mathcal{A}), \end{aligned} \quad (19)$$

where  $\mathcal{A} \subset \mathcal{A}_r(u_n) = \{x \in \mathcal{F}^{\xi, a_n, b_n} : r(x) \geq u_n\}$ ,  $1\{\cdot\}$  is the indicator function,  $u_n = r(b_n) + u r(a_n)$  for some  $u \geq 0$  is a high quantile of  $r(X)$ , and we model the probability of the event  $\{r(X) > u_n\}$  using an appropriate regression formulation.

Let  $x_j \in \mathbb{R}_+^L$  ( $j = 1, \dots, n$ ) be independent realizations of a generalized regularly varying stochastic process  $X$  observed at locations  $s_1, \dots, s_L \in S$ . The log-likelihood function for the model (19) based on the  $r$ -exceedances over the threshold  $u_n$  among  $x_1, \dots, x_n$  is

$$\mathcal{L}_{\text{Thres}}(\theta) = \log \Pr(N_{u_n} = n_{u_n}) + \sum_{j \in K_{u_n}} \log f^r(x_j), \quad (20)$$

where  $N_{u_n}$  is the random number of exceedances,  $K_{u_n} = \{j \in 1, \dots, n : r(x_j) \geq u_n\}$  contains the indexes of the  $n_{u_n}$   $r$ -exceedances over  $u_n$ , and  $f^r$  is the finite-dimensional density function of a generalized  $r$ -Pareto process sampled at locations  $s_1, \dots, s_L$ , i.e.,

$$f^r(x) = \frac{\lambda \left[ \{1 + \xi(x - b_n)/a_n\}_+^{1/\xi} \right]}{\Lambda(\mathcal{A}_r)} \prod_{l=1}^L a_n(s_l)^{-1} \left\{ 1 + \xi \frac{x(s_l) - b_n(s_l)}{a_n(s_l)} \right\}_+^{1/\xi - 1}, \quad x \in \mathcal{A}_r(u_n), \quad (21)$$

where  $\Lambda(\mathcal{A}_r) = \int_{\mathcal{A}_r} \lambda(x) dx$  and  $\mathcal{A}_r$  is defined in (10). The second term on the right-hand side of (21) is the Jacobian for the marginal transformations from the generalized Pareto scale used for the data to the unit Fréchet scale on which the dependence model is defined.

A model for  $N_{u_n}$  must be specified. In similar contexts Wadsworth and Tawn (2014) and Engelke et al. (2015) use a Poisson distribution suggested by the relationship with block

maxima, yielding log-likelihood function

$$\mathcal{L}_{\text{Pois}}(\theta) = -\log n_u! + n_u \log \Lambda(\mathcal{A}_r) - \Lambda(\mathcal{A}_r) + \sum_{j \in K_{u_n}} \log f^r(x_j), \quad (22)$$

but the Pareto methodology accommodates other models. Thibaud and Opitz (2015), for instance, suppose that  $N_u$  is fixed and use a binomial distribution, which is easily linked to the Poisson point process model. These approaches presuppose that the probability of observing an exceedance does not depend on explanatory variables, but if it does then a binary classifier such as logistic regression can be used to model how the probability of observing an extreme event varies, as in Section 6.3.

Maximization of (20) or (22) can be difficult and we recommend first estimating the marginal parameters  $\xi$ ,  $a'_n$ ,  $A$ ,  $b'_n$  and  $B$  and then fitting a dependence model by fixing the marginal parameters at their estimates. The marginal parameters can be estimated by maximizing the independence log-likelihood,

$$\begin{aligned} \ell_{\text{indep}}(\xi, a'_n, b'_n, \theta_A, \theta_B) \\ = \sum_{j=1}^n \sum_{l=1}^L 1\{x_j(s_l) \geq b_n(s_l)\} \log \left[ \frac{1}{a_n(s_l)} \left\{ 1 + \xi \frac{x_j(s_l) - b_n(s_l)}{a_n(s_l)} \right\}^{-1/\xi-1} \right], \end{aligned} \quad (23)$$

$$\xi \in \mathbb{R}, \theta_A \in \Theta_A, \theta_B \in \Theta_B,$$

under the constraint  $r(b_n) = u_n$ , with parameter uncertainty assessed by resampling the  $x_j$ . Any other inference procedure allowing a common shape parameter could also be employed.

One way to estimate the dependence parameters is to minimise the function

$$\ell_{\text{extr}}(\theta) = \sum_{l, l'=1, \dots, L} \{\hat{\pi}(s_{l'}, s_l) - \pi_{\theta_W}(s_{l'}, s_l)\}^2, \quad (24)$$

where  $\hat{\pi}$  denotes an estimate of (17), such as that obtained by replacing exceedance proba-

bilities by the corresponding frequencies (Davis et al., 2013),

$$\hat{\pi}(s_{l'}, s_l) = \frac{\sum_{j=1}^n 1\{x_j(s_{l'}) \geq b_n(s_{l'}), x_j(s_l) \geq b_n(s_l), r(x_j) \geq u_n\}}{\sum_{j=1}^n 1\{x_j(s_l) \geq b_n(s_l), r(x_j) \geq u_n\}}.$$

This approach is robust and ensures that the fitted model has the same average number of locations jointly exceeding the threshold function  $b_n$  as in the data base, but uncertainty quantification for the resulting estimates is not straightforward.

Maximum likelihood estimation of  $\theta_W$  has been studied for specific risk functionals but often performs poorly because the limiting process is misspecified for finite  $u_n$  (Engelke and Malinowski, 2014; Huser et al., 2016). Alternatives involve censoring of low components (e.g., Wadsworth and Tawn, 2014), composite likelihoods (Padoan et al., 2010; Huser and Davison, 2013; Castruccio et al., 2016) or M-estimation using pairwise tail indexes (Einhorn et al., 2016a,b). All are more robust to mis-specification but work only for specific risk functionals and are dimensionally limited, either by the computational burden due to the numerical evaluation of the scaling constant  $\Lambda(\mathcal{A}_r)$  and the censoring, or, for pairwise procedures, by combinatorial considerations. Efficient algorithms for censored likelihood are available (de Fondeville, 2016) and tractable for  $L$  up to a few hundred dimensions for the angular processes corresponding to the Brown–Resnick and extremal  $t$  models. Gradient scoring (de Fondeville and Davison, 2018) can be applied to a large class of risk functionals and avoids the computation of  $\Lambda(\mathcal{A}_r)$ , making inference tractable for  $L$  in the thousands: for log-Gaussian random functions, its numerical complexity is that of matrix inversion. These could also be used to estimate the entire vector of parameters  $\theta$  simultaneously, thereby allowing a full quantification of the uncertainties, for instance by resampling.

## 5 Model validation

Suppose that we have an estimate  $\hat{\theta}$  of (18) and a measure of its uncertainty and we wish to check the quality of the fitted model.

The marginal tail behaviour at each sampled location  $s_1, \dots, s_L$  can be checked by comparing the observations with the fitted marginal model. Let  $u_q(s_l)$  denote the empirical  $q$  quantile of the  $r$ -exceedances at  $s_l$ , estimated using only observations  $x_j$  for which  $r(x_j) \geq u_n$ , where  $q$  has been chosen such that  $r(u_q) \geq u_n$ , and let  $n_q$  denote the number of the  $x_j$  exceeding  $u_q(s_l)$ . Following equation (14), we have

$$\Pr \{X(s_l) - u_q(s_l) \geq x \mid X(s_l) \geq u_q(s_l)\} \approx H_{\hat{\xi}, \hat{\sigma}(s_l)}(x), \quad x \geq 0,$$

with  $\hat{\sigma}(s_l) = \hat{a}'_n \hat{A}(s_l) + \hat{\xi} \{u_q(s_l) - \hat{B}(s_l) - \hat{b}'_n \hat{A}(s_l)\}$ , and we can use this to check the marginal fit. Pointwise confidence intervals for QQ-plots can be obtained by resampling: we draw  $m$  samples of size  $n_q$ ,  $(Z_1^1, \dots, Z_{n_q}^1), \dots, (Z_1^m, \dots, Z_{n_q}^m)$  from the fitted distribution and let  $Z_{(j)}^1, \dots, Z_{(j)}^m$  denote the  $j$ th order statistic of each sample. A 95% confidence interval for the generalized Pareto fit is then defined as the 2.5 and 97.5 empirical percentiles of  $Z_{(j)}^1, \dots, Z_{(j)}^m$ . When the estimator used to obtain  $\hat{\theta}$  is asymptotically normal, estimation uncertainty can be taken into account to some extent by drawing the  $m$  samples from different generalized Pareto distributions whose parameters are normally distributed with means  $\hat{\xi}$  and  $\log \hat{\sigma}(s_l)$  respectively and covariance matrix corresponding to the uncertainty of  $\hat{\theta}$ .

The dependence model can be assessed by comparing the fitted extremogram with the corresponding empirical values of (17). If the model is stationary and isotropic, then  $\pi$  depends only the distance  $h$  between two locations, and it can be plotted as a function of the distance, and if relevant, the orientation, of the two locations. For an anisotropic model it is preferable to map how the dependence varies with the spatial coordinates, as in Figure 9.

Model comparison can be performed using the Akaike or composite likelihood information criteria (Davison and Gholamrezaee, 2012), and formal comparison of nested models can be based on scoring rules (Dawid et al., 2016; de Fondeville and Davison, 2018). A relative root mean squared error or the continuous ranked probability score (Gneiting and Raftery, 2007) can be used to assess the predictive performance of the model. An empirical probabilistic

forecast can be issued by simulating from the fitted model conditioned on the observations, which is equivalent to conditional simulation of a Gaussian process when the angular process is log-Gaussian.

We illustrate the application of these ideas in the next two sections.

## 6 Modelling Extreme European Windstorms

On 25 January 1990 the windstorm Daria, one the severest extra-tropical cyclones ever observed, struck the United Kingdom. Over that day and the next, 97 deaths were reported and damage valued at around 8.2 billion dollars occurred. The strongest measured gusts were  $47.2 \text{ m.s}^{-1}$ , equivalent to a category 1 hurricane. Figure 3 shows the maximum speed over three-hour intervals of the wind gusts sustained for at least 3s for the 24 hours during which the storm peaked over the UK. To give an idea of the severity of this storm, damaging windspeeds are considered to start at  $25 \text{ m.s}^{-1}$  (Roberts et al., 2014). About ten years later, on 26 December 1999, storm Lothar swept across western and central Europe. A wind speed of  $46.9 \text{ m.s}^{-1}$  was recorded in Paris, and the weather station at the summit of the ‘Dole’ in Switzerland recorded a maximum wind gust of  $55.9 \text{ m.s}^{-1}$ . Lothar, equivalent to a category 2 hurricane, caused 8 billion dollars of losses and more than 100 deaths.

These two events illustrate why estimating the risk linked to such natural hazards has become a major question in recent decades, especially as the possible influence of global warming is far from understood.

### 6.1 Risk estimation for extreme windstorms

Risk estimation for extreme windstorms has generally been limited to the use of historical catalogues of events to test the resilience of infrastructure (Haylock, 2011; Pinto et al., 2012), but unfortunately such storms are rare and the catalogues usually span only 40 to 50 years. Further events can be generated by statistical perturbation of the wind field intensity, shape

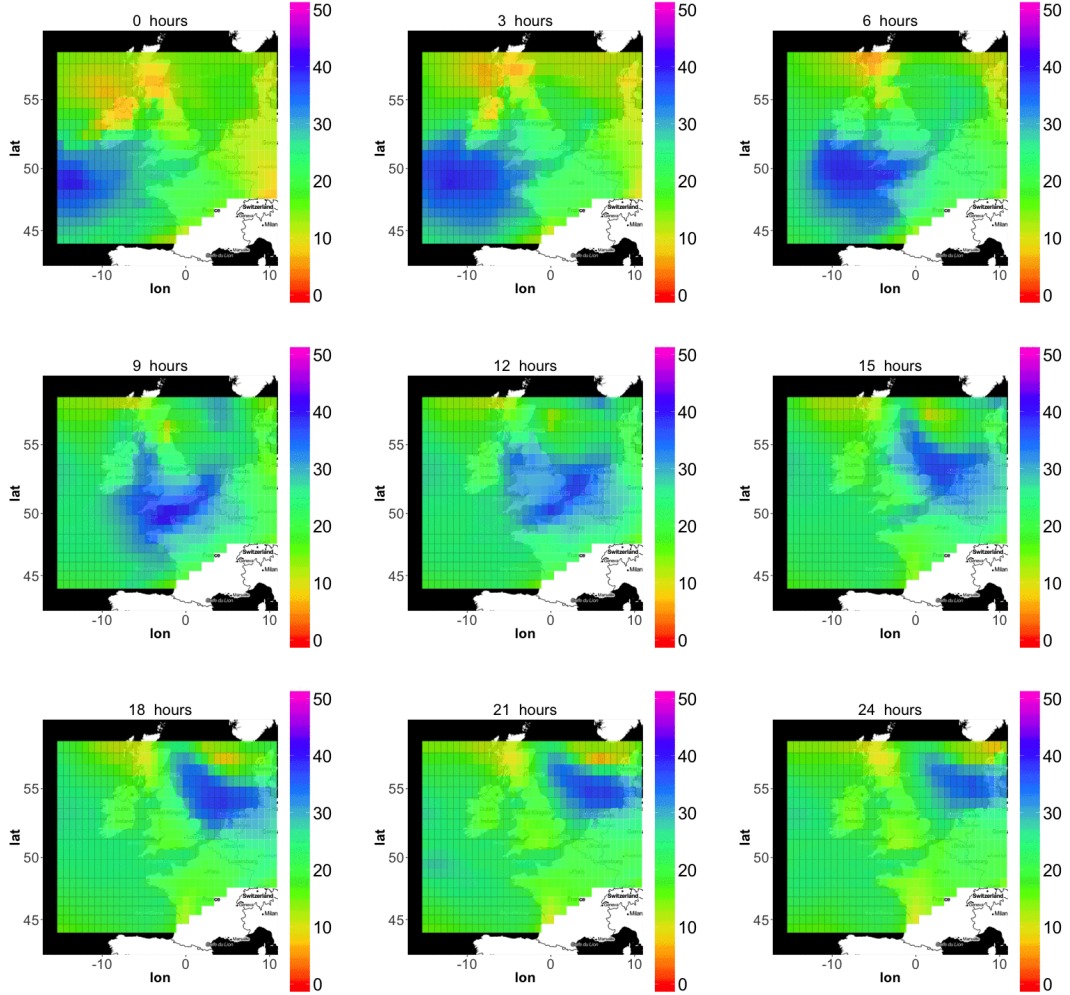


Figure 3: Maximum speed ( $\text{m.s}^{-1}$ ) over the past  $3h$  hours of the wind gusts sustained for at least 3s from ERA-Interim reanalysis during the peak of windstorm Daria, which swept over Europe during January 1990.

and location (Hall and Jewson, 2008) or by detecting storms in multiple numerical climate outputs (Della-Marta et al., 2010). In both cases the same storms may be re-cycled but with differing climatological indexes because of different hypotheses and approximations used by the models. Yiou (2014) instead proposed to create new storms from historical catalogues by reordering time steps based on spatial analogues. Uncertainties and bias linked to all these approaches are likely to be large and difficult to estimate, and studies on climatological projections have stressed their inability to accurately reproduce extreme events (e.g., Weller



et al., 2013). All these methods generate storms whose tail behaviour cannot be extrapolated to still rarer events.

Extreme value theory was applied to the problem by Della Marta and Mathis (2008), who performed a POT analysis on univariate summaries characterizing extreme windstorms, but they ignore spatial dependence. Ferreira and de Haan (2014) suggest how historical windstorm records might be extrapolated to higher intensities using Pareto processes, but their approach cannot generate new storms. Economou and David (2014) adapted Bayesian hierarchical models to extra-tropical cyclones, but included dependence using covariates such as mean sea level pressure, which limits the capacity of the model to generate new patterns and intensities. The previous work closest to ours is Sharkey et al. (2020), who use a Lagrangian approach to model the tracks and severity of European windstorms. Their model for storm tracks is more detailed than ours, but their dependence structure is based on a non-extremal model and neglects the temporal element.

We propose an approach based on generalized  $r$ -Pareto processes, which extends the Della Marta and Mathis (2008) approach to allow not only local risk estimation but also the generation of new extreme events that are spatially and temporally consistent.

## 6.2 Data set and region of study

To build our stochastic weather generator, we follow the methodology of the extreme windstorms (XWS) catalogue (Roberts et al., 2014), which provides historical records of the 50 most extreme storms over Europe for winters from 1979 to 2014; more precisely it contains maps of 72-hour maximum wind gusts over northern Europe. In this catalogue, the ‘extreme storms’ are chosen to focus on events with high impact on infrastructure; indeed, storms with the highest maximum wind speeds overall need not do the most damage, as they may not pass over inhabited areas. To apply our methods we must define univariate summaries that characterise the most damaging events.

The XWS catalogue tracks storms in the ERA-Interim reanalysis (Dee et al., 2011),

a real-time climate model whose records start in 1979, and provides time series for many climatological indexes. In particular for each three-hour period it provides the maximum speed of the wind gusts sustained for at least 3s; see Figure 3. The model is run every six hours on a grid whose cells are squares with sides that can be chosen between  $3^\circ$  and  $0.125^\circ$ ; the native size is  $0.75^\circ$ , with other resolutions obtained by interpolation. In addition to the 6-hourly fields obtained by data assimilation, i.e., by constraining the grid values to station measurements, 256-hour forecasts are generated each day at 00UTC and 12UTC, and can be used to obtain a three-hourly database. Most European winter storms evolve quickly and last only for a short period, so such a fine time resolution is necessary.

Our study focuses on the region  $S$  with boundaries N57.75, S44.25, E25 and W10.5; see Figure 4. The reanalysis model is known to have a systematic bias over regions with rapid variations in altitude (Donat et al., 2011), so mountainous regions such as the Pyrenees and the Alps have been dropped from  $S$ , leaving an incomplete grid with 605 cells based on the native resolution of  $0.75^\circ$ . Similarly to the XWS catalogue methodology, we combined the maximum wind gust sustained for at least 3s from the reanalysis with the forecasts to obtain a three-hourly spatial time series. Extra-tropical windstorms over Europe occur only during the winter, so the study period is restricted to October–March.

### 6.3 Storm definition and frequency modelling

Following Roberts et al. (2014) and Vautard et al. (2019), we define a storm as the exceedance of the spatial average over a region with very dense infrastructure during a 24-hour period. The spatio-temporal process  $X(s, t)$  represents the wind field at location  $s \in E \subset \mathbb{R}^2$  and time  $t \in T = (1979, 2014)$ . We define the risk functional  $r$  at time  $t$  to be the spatial average

$$r(x)(t) = |E_{\text{ABLP}}|^{-1} \int_{E_{\text{ABLP}}} x(s, t) \, ds, \quad s \in E, \quad t \in T,$$

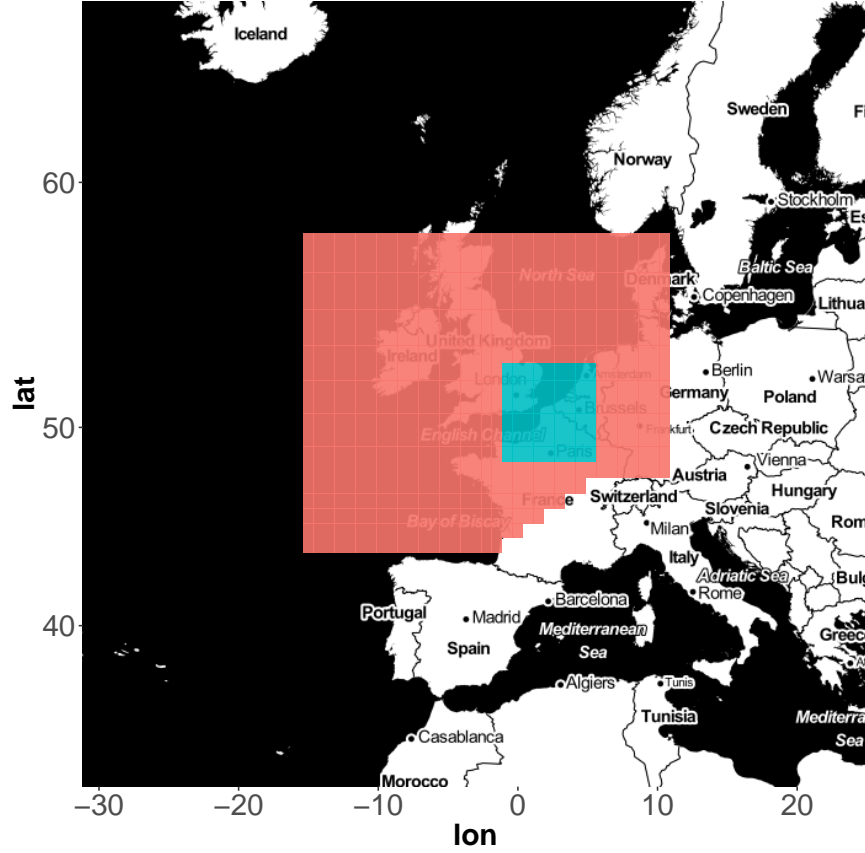


Figure 4: Area of study (coloured cells) for modelling extreme windstorms over Europe. Mountainous regions were removed to avoid the systematic bias of the reanalysis model. The green cells show the region  $E_{ABLP}$  containing Amsterdam, Brussels, London and Paris.

where  $E_{\text{ABLP}}$  is the green region in Figure 4, which includes Amsterdam, Brussels, London and Paris. To suppress the temporal clustering of high values of  $r(x)(t)$ , we centre the time frame on the largest spatial average for each event and keep only events that are at least 48 hours apart, yielding  $n = 1561$  observations. Storm Daria corresponds to a maximum intensity of  $r(x) = 32.1\text{m.s}^{-1}$ .

Our model is based on the approximation (19), in which three components must be modelled: the distribution of the indicator variable  $1\{r(X) \geq u_n\}$ ; the margins, which include a tail index  $\xi$  and the functions  $a_n$  and  $b_n$ ; and the dependence structure of the generalized  $r$ -Pareto process  $P$ .

To model the probability of observing an  $r$ -exceedance, for simplicity we choose  $u = 0$  such that  $r$ -exceedances are defined as events for which  $r(X) \geq r(b_n)$ ; see the comments after (19). A natural choice for  $u_n = r(b_n)$  is then a high quantile of the random variable  $r(X)$ . In order to include most of the XWS storms in our set of exceedances, we take  $u_n = q_{0.96}\{r(X)\} = 24\text{m.s}^{-1}$ , yielding 63 events for the period 1979 to 2014. This quantile also corresponds to a stability region in the estimated tail index for the scalar  $r(X)$ . The risk functional, the  $r$ -exceedances and the XWS storms are shown in Figure 5. The 63 events, depicted by the red dots, coincide with most of the windstorms from the XWS catalogue represented by the vertical lines, so the exceedances of the risk functional  $r$  successfully characterise extreme windstorms hitting the region  $E_{\text{ABLP}}$ . The events in the catalogue that do not match large values of  $r$  mostly pass over southern regions of Europe.

Figure 5 also shows that the temporal distribution of  $1\{r(X) \geq u_n\}$  is non-stationary. The impact on windstorms of climatic circulation patterns such as the North Atlantic Oscillation index (NAO) has been underscored in several studies (Donat et al., 2010; Pfahl, 2014), so we use logistic regression to model the influence of potential explanatory variables.

We extracted the 3-hourly mean sea level pressure from the ERA-interim reanalysis and computed the NAO using its definition in terms of empirical orthogonal functions (EOF) (Blessing et al., 2005), as the first eigenvalue of the mean sea level pressure anomaly at

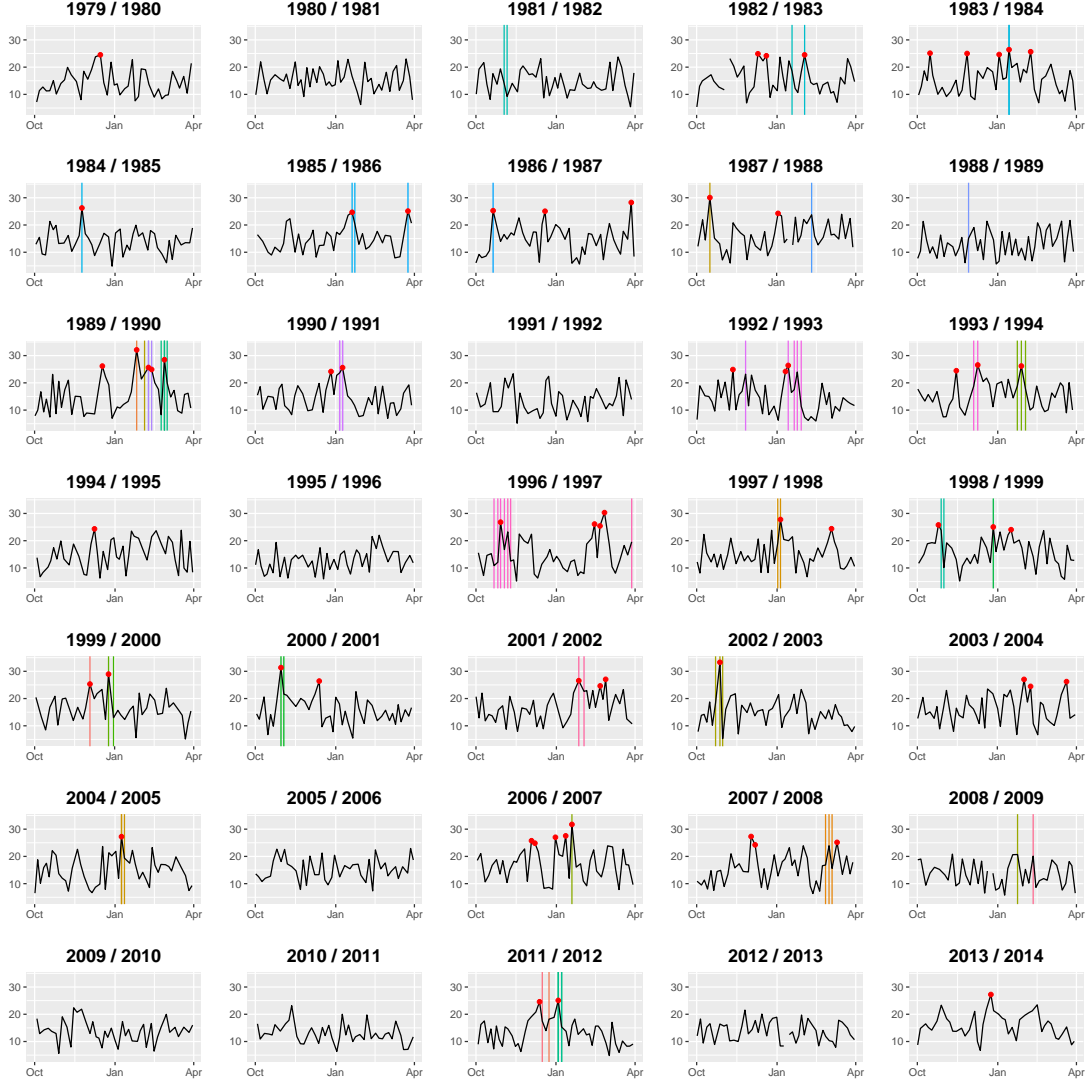


Figure 5: Declustered risk functional  $r(X)(t) = |E_{ABLP}|^{-1} \int_{E_{ABLP}} X(s, t) ds$  ( $\text{m.s}^{-1}$ ), computed on the ERA–Interim data set for each winter.  $r$ -exceedances above the empirical 0.96 quantile are represented by red dots and windstorms from the XWS catalogue are represented by vertical lines coloured by dates.

a given time  $t$ . We likewise computed the Antarctic Oscillation index (AAO) and created indexes for temperature anomalies based on EOFs. Time was also included as a potential covariate.

An analysis of deviance reveals that the NAO index and the first and third eigenvalues of the temperature anomaly affect the occurrence of winter storms at the 0.1% significance level.

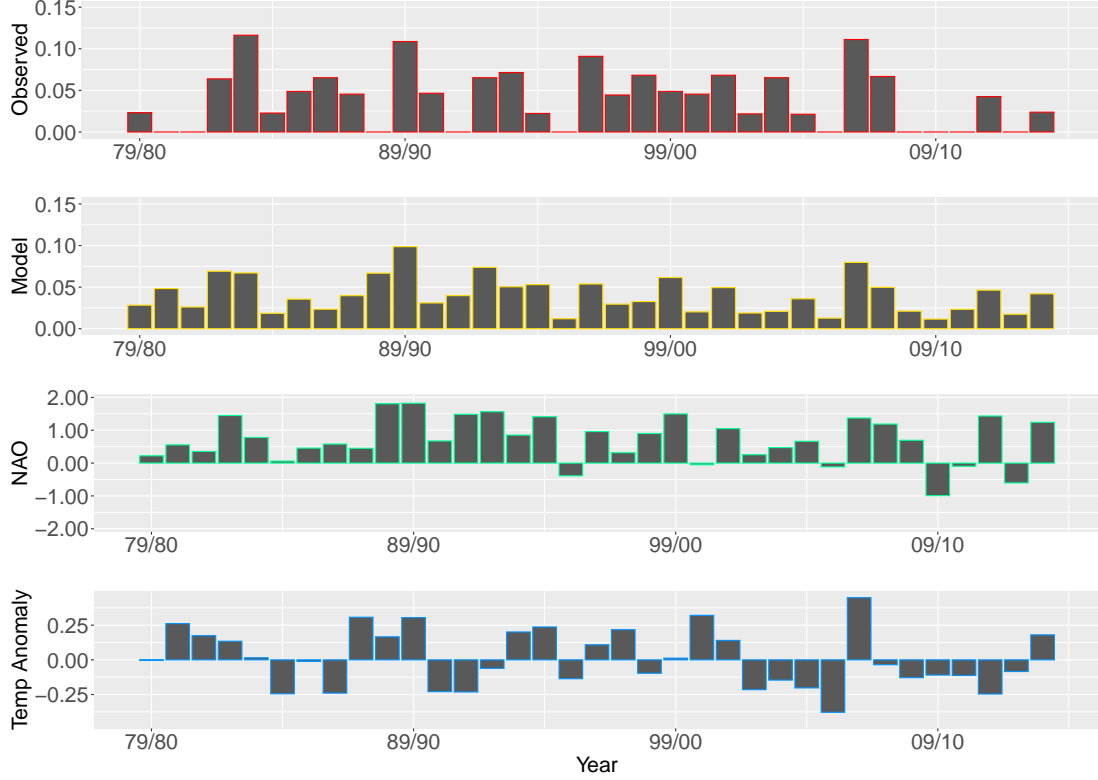


Figure 6: Annual summary of the model for the probability of storm occurrence: Observed frequency (top), modelled frequency (second row), North Atlantic Oscillation index (third row) and aggregated temperature anomaly indexes (bottom).

Figure 6 summarises the fit of the model. Plots at a daily scale are shown in Appendix D.

## 6.4 Marginal model

Fitting the marginal model involves the estimation of a tail index  $\xi \in \mathbb{R}$  and the functions  $a_n$  and  $b_n$  under the assumptions of Section 3. In general, a parametric model for the functions  $A$  and  $B$  might be necessary, as in Engelke et al. (2019), but for simplicity we allow them to vary separately at each grid cell, i.e.,  $A(s_l) = A_l > 0$  and  $B(s_l) = B_l \in \mathbb{R}$  for each location  $s_l$  ( $l = 1, \dots, 605$ ).

With the model for the probability of storm occurrence in Section 6.3, the parameter  $b'_n = r(b_n)$  is fixed to the 0.96 empirical quantile of the series  $r(X)$ . The threshold-stability of generalized Pareto distributions does not allow us to identify the function  $B$  without

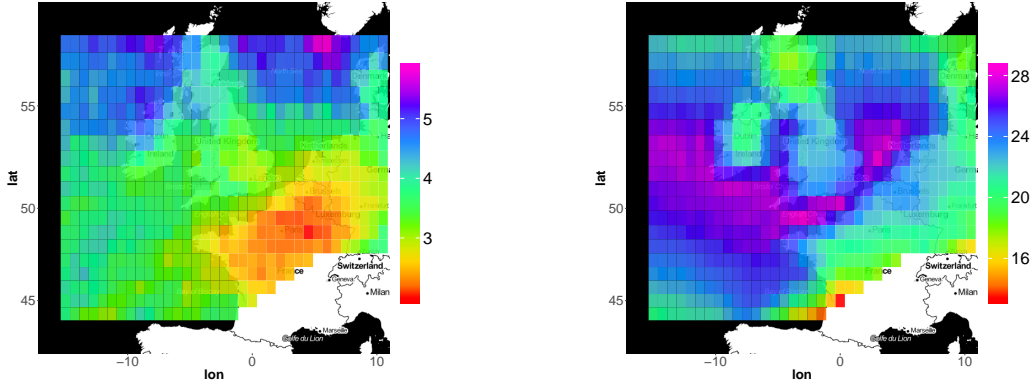


Figure 7: Estimated functions  $A$  (left) and  $B$  (right) of the generalized  $r$ -Pareto process for modelling extreme windstorms over Europe. Estimates are obtained by shifting the local empirical quantiles  $u_{0.675}\{X(s_l)\}$  by  $b'_n = 24\text{m.s}^{-1}$ .

further hypotheses, so we assume that  $r(B) = 0$  and thus set

$$B_l = u_{q'}\{X(s_l)\} - b'_n, \quad l = 1, \dots, 605,$$

where  $u_{q'}\{X(s_l)\}$  is the empirical  $q'$  quantile of the  $r$ -exceedances above threshold  $u_n$  at location  $s_l$ , with  $q'$  chosen so that  $r(B) = 0$  to enforce identifiability. For our data set, we find  $q' = 0.675$ , yielding 184 marginal excesses and estimated location function  $\hat{B}$  shown in Figure 7. Standard errors for  $\hat{B}$ ,  $\hat{A}$  and  $\hat{\xi}$  can be obtained by resampling.

For tractability we first fit the marginal model, estimating the tail index  $\xi$  and the scale parameters  $a_l > 0$  ( $l = 1, \dots, 605$ ) by maximizing the independence log-likelihood (23). For a given tail index  $\xi$ , the likelihood for the exceedances above the threshold  $b_l$  is optimized independently for each  $s_l$  ( $l = 1, \dots, L$ ). As exceedances from the same storm correspond to the same overall event, we weight each log-likelihood contribution inversely proportionally to the number of exceedances in the storm from which it arises, so that each storm affects the estimates roughly equally. This yields the maximum independence likelihood estimate  $\hat{\xi} = -0.15_{0.01}$ ; the corresponding estimated scale function  $\hat{A}$  is shown in Figure 7.

Figure 8 displays QQ-plots of the local tail distribution at six locations. The overall fit of the marginal model is convincing, as the observations mostly remain within the confidence

intervals. The quality of the model fit for the distribution of  $r(X)$  above the threshold  $u_n$  also seems to be adequate. The standard independence likelihood estimates led to a poor fit for  $r(X)$ , whereas the model obtained with the re-weighting procedure is plausible.

## 6.5 Dependence model

Following equation (19), we model the storms by a generalized  $r$ -Pareto process with state space  $S = E \times [0, 24]$  and whose dependence structure must be specified. For the angular component  $W_{\xi,A}$ , we choose a process with log-Gaussian random functions and Whittle–Matérn semi-variogram (Whittle, 1954, 1963; Matérn, 1960)

$$\gamma(s, s', t, t') = \kappa \{1 - \|h\|^\nu K_\nu(\|h\|)\}, \quad \kappa, \nu > 0, \quad (25)$$

where  $K_\nu$  is the modified Bessel function of the second kind of order  $\nu$ , and (Gelfand et al., 2010, pp. 428, 432)

$$\|h\| = \|h(s, s', t, t')\| = \left\{ \left\| \frac{\Omega(s' - s) - V(t' - t)}{\tau_s} \right\|_2^2 + \left| \frac{t' - t}{\tau_t} \right|^2 \right\}^{1/2}, \quad s, s' \in S, t, t' \in \{0, 3, \dots, 24\}, \quad (26)$$

with positive scale parameters  $\tau_s$  and  $\tau_t$  for the space and time dependence, a wind vector  $V \in \mathbb{R}^2$  that models the average displacement of the storm in a three-hour period, and an anisotropy matrix

$$\Omega = \begin{bmatrix} \cos \eta & -\sin \eta \\ a \sin \eta & a \cos \eta \end{bmatrix}, \quad \eta \in \left(-\frac{\pi}{4}, \frac{\pi}{4}\right], \quad a > 0,$$

to allow the spatial dependence in (26) to decrease faster in a particular direction. Estimation of  $\nu$  is difficult, so we set  $\nu = 1$ , which would allow the use of more flexible non-stationary models such as that of Fuglstad et al. (2015).

The semi-variogram function (25) is motivated by an exploratory analysis in which the



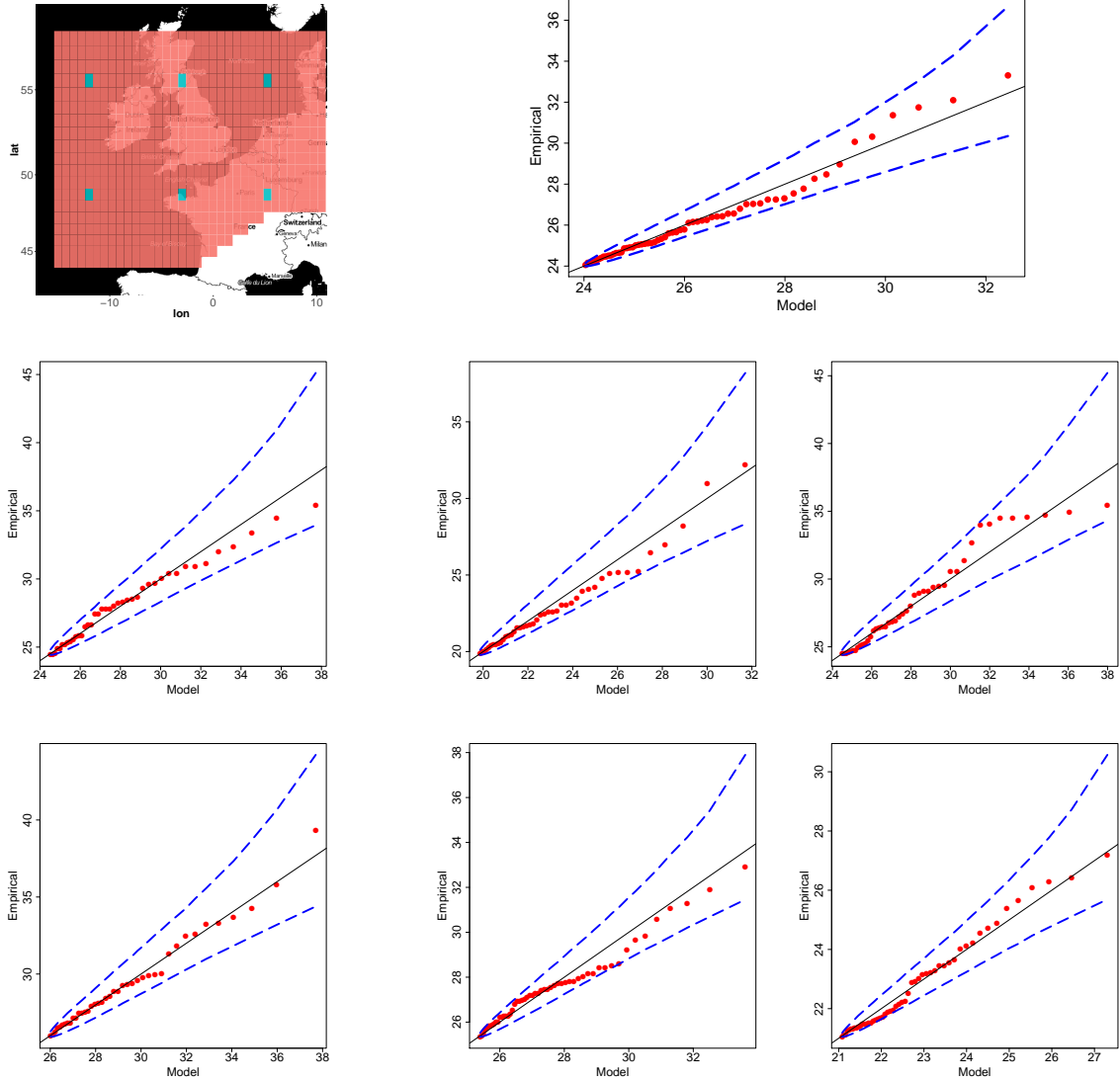


Figure 8: Model assessment for the windstorm data. The lower six panels show QQ-plots of the local tail distributions for the locations represented by the green cells in the map at the upper left. The thresholds correspond to the local 0.675 quantiles of the  $r$ -exceedances, yielding 184 excesses for each cell. The upper right panel QQ-plot is for exceedances of  $r(X)$  above the threshold  $u_n = 24 \text{ m.s}^{-1}$  modelled by a generalized Pareto distribution with scale  $\hat{a}'_n$  and tail index  $\hat{\xi} = -0.15$ . The blue dashed lines corresponds to pointwise 95% confidence intervals.

Table 1: Semi-variogram parameter estimates obtained by minimizing (24) and using the gradient score. The standard deviations (subscripts) are obtained using a block jackknife.

	$\kappa$	$\tau_s(\text{km})$	$\tau_t(\text{h})$	$a$	$\eta(^{\circ})$	$V_1(\text{km.h})^{-1}$	$V_2(\text{km.h}^{-1})$
Least squares	3.6	623	87.3	0.7	-4.12	49.3	15.5
Gradient score	2.85 <sub>0.01</sub>	337 <sub>11.6</sub>	91.3 <sub>7.7</sub>	0.68 <sub>0.01</sub>	21.2 <sub>0.1</sub>	50.4 <sub>2.9</sub>	12.5 <sub>1.7</sub>

space-time extremogram

$$\pi(h_s, h_t) = \Pr\{X(s', t') \geq u' \mid X(s, t) \geq u\}, \quad h_s = s' - s \in S, \quad h_t = t' - t \in \{0, 3, \dots, 24\},$$

with thresholds  $u, u'$  at local 0.675 empirical quantiles of the set of  $r$ -exceedances, is estimated using the empirical estimator for the probabilities described in Section 4; see Figure 9.

We used both the least squares and gradient scoring procedures to estimate the parameters of (25). We applied gradient scoring using a composite approach with 100 random subsets using the same 50 locations for every storm, since we found this to be more robust than including all locations; in general we recommend using subsets whose size is roughly the same as the number of samples.

Table 1 shows the parameter estimates, and the extremal dependence models are displayed in Figure 9. The fits agree on the strength of dependence at long distances and are consistent overall with the empirical values, but differ for the anisotropy: while the least squares fit picks out the long-range north-east anisotropy, the gradient score captures the short-range south-east anisotropy. This change in direction cannot be captured by our rather simple model. The estimated wind vectors  $\hat{V}$  are similar and are consistent with the observation that storms are born over the Atlantic and usually move towards the North Sea in an east-north-easterly direction. The overall fits look reasonable, with a slight under-estimation of temporal dependence for the scoring approach.

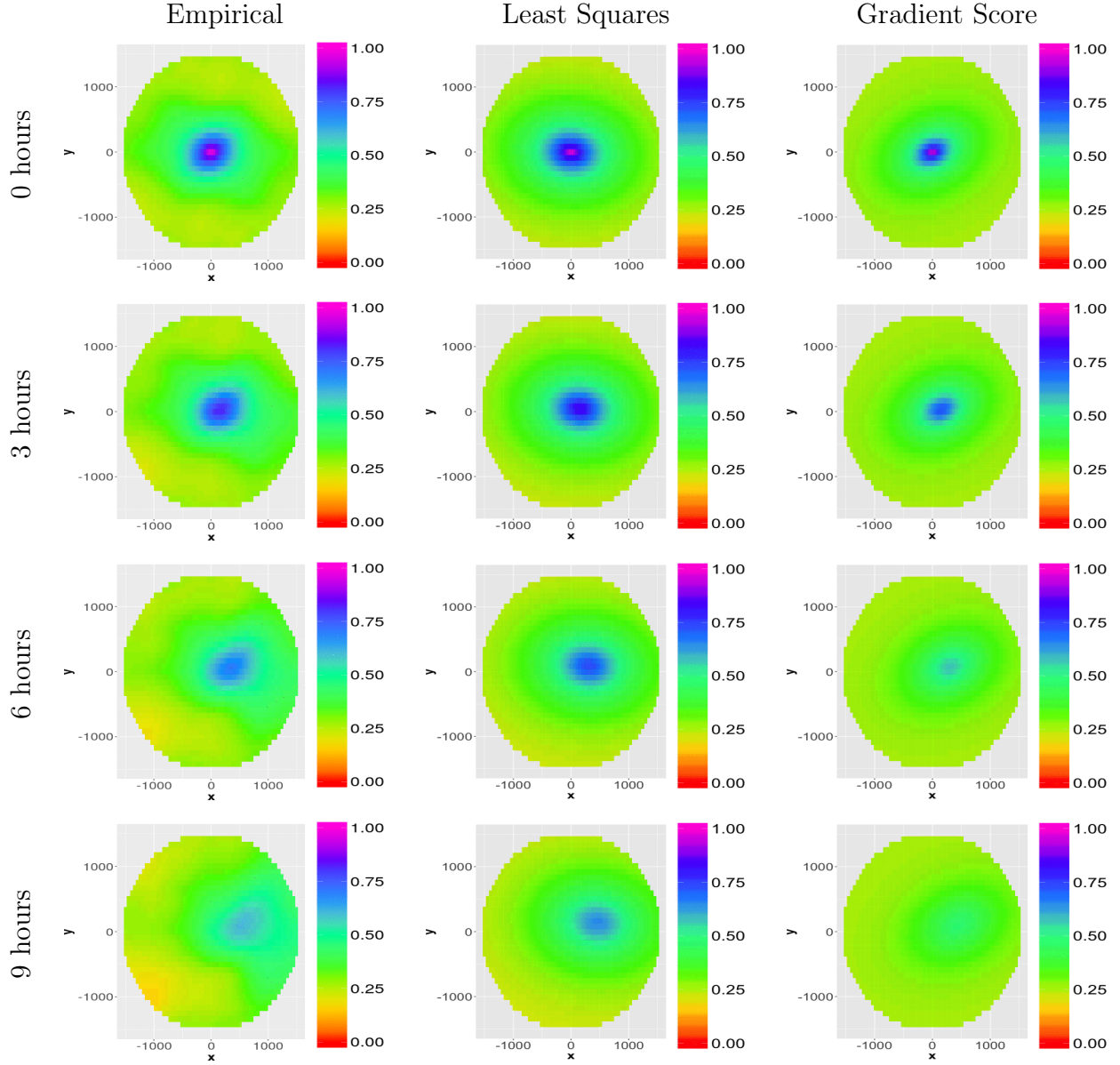


Figure 9: Extremograms as functions of distance (km): empirical estimates (left), fitted values obtained using the parameters from least squares (middle) and gradient scoring (right) estimates. Each row represents a 3-hour time step.

## 6.6 Simulations

The usefulness of our model can be checked by simulating extreme storms from it, using a version of Algorithm 1 modified to ensure that the maximum spatial average occurs at  $t = 12$  hours, consistent with our definition of an extreme storm. First the angular component of

the spatial process at time  $t = 12$  is simulated. Then we iteratively simulate the remaining time steps by consecutively generating the spatial process at times  $t = 9, 6, 3, 0, 15, 18, 24$  conditionally on the variables already simulated. If the new time step yields a spatial average greater than its value at time  $t = 12$ , the sample is rejected and the procedure is repeated until a suitable candidate is found.

For an angular process with log-Gaussian random functions, such a simulation algorithm is equivalent to conditional simulation of multivariate Gaussian random vectors. Figure 10 shows a simulated storm with intensity  $r(X) = 29.1\text{m.s}^{-1}$ , similar to that of Daria. The images are rougher than those in Figure 3 but nevertheless seem visually convincing.

## 7 Flood risk assessment

In August 2005, the city of Zurich suffered from heavy floods that led to estimated property damage of around 3 billion Swiss francs and six deaths (Bezzola and Hegg, 2007). Zurich is especially risk-prone, as it lies at the foot of a lake and is traversed by several rivers, including the Sihl, which flows under the city's main railway station. Although the 2005 event was not caused by unusually a high water level of the Sihl (Jaun et al., 2008), it triggered an overall assessment of flood risk for the city. An extreme discharge of this river could cause hundreds of millions of francs of losses by damaging infrastructure and by preventing half a million commuters from travelling. A good understanding of the risk related to high levels of the Sihl is thus crucial to consideration of mitigation measures. Below we use our ideas to construct a stochastic generator of extreme rainfall over the Sihl river basin, in order to create a catalogue of events for input to hydrological models. Cloke and Pappenberger (2009) review similar approaches based on climate models.

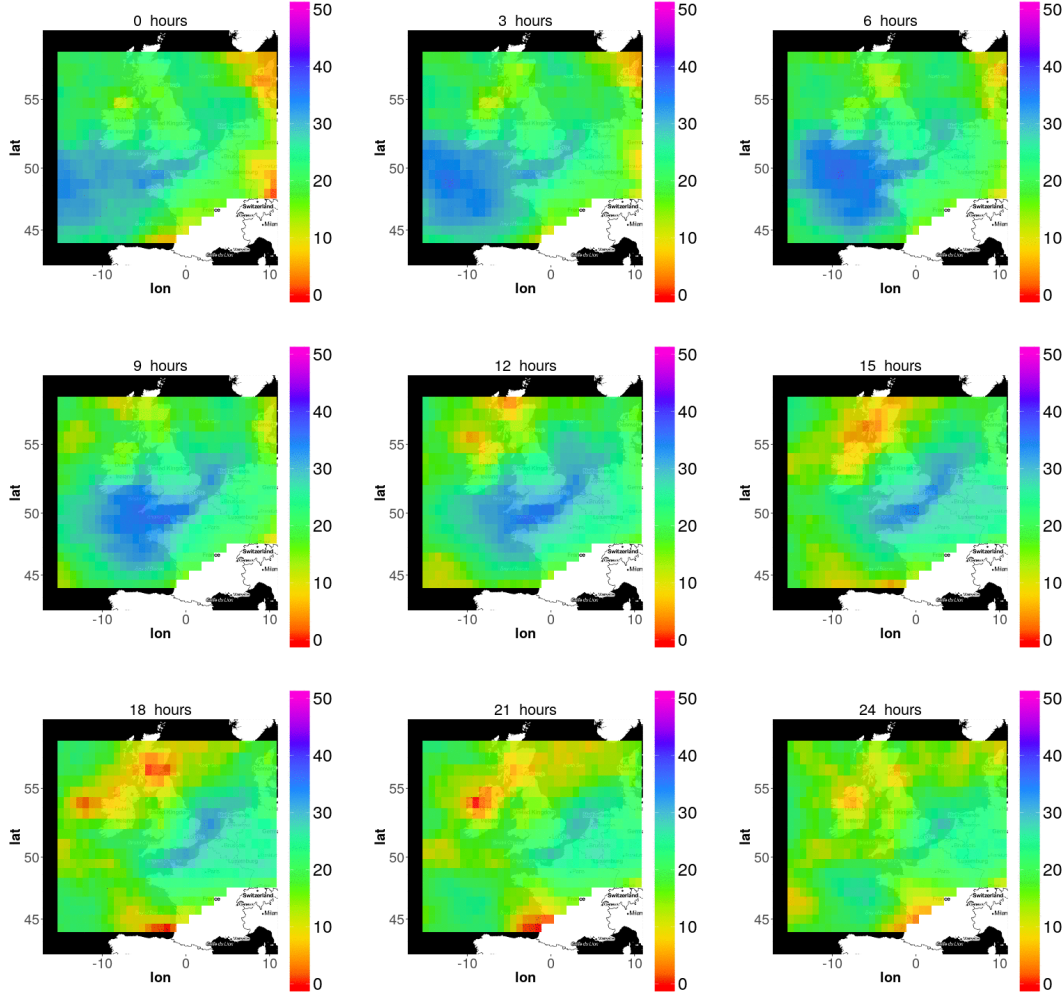


Figure 10: Simulated maximum speed ( $\text{m.s}^{-1}$ ) over the past  $3h$  hours of wind gusts sustained for at least 3s. The storm has an intensity  $r(X) = 29.1 \text{ m.s}^{-1}$ .

## 7.1 Data set and region of study

Figure 11 shows the region of study, a rectangle south-west of Zurich including the Sihl river basin. Any rain falling in the green area can be expected to flow under the station. Rainfall is the result of various physical processes, including cyclonic and convective regimes, which can usually only be distinguished using high resolution data such as radar measurements. In this study we use the CombiPrecip data set produced by MeteoSwiss (Sideris et al., 2014; Gabella et al., 2017; Panziera et al., 2018), which provides an estimate of the hourly accumulated rainfall over Switzerland from 2013 to 2018. Owing to changes in acquisition and processing

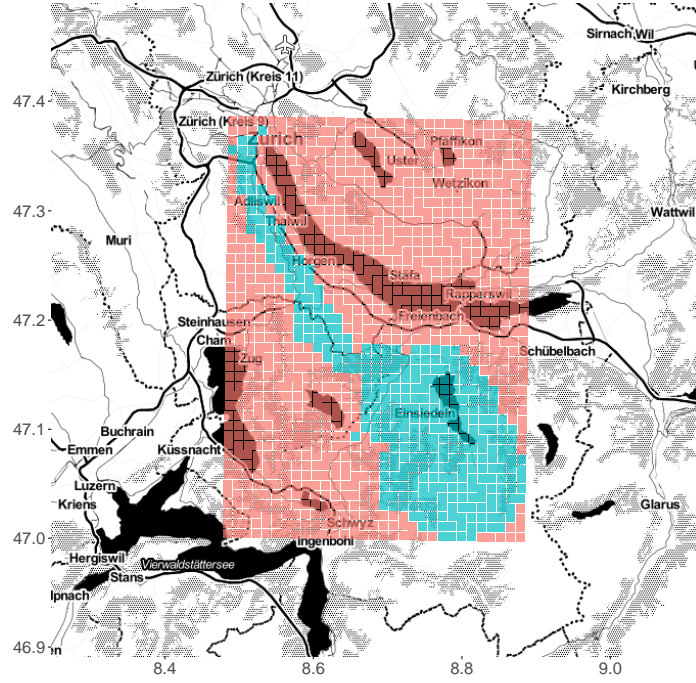


Figure 11: Sihl river basin (green) and study region (red).

in 2013, earlier measurements are inconsistent with more recent data, but even with this reduced temporal frame the data set includes  $n = 52,413$  radar images. The Sihl river basin is orographically homogeneous and is located at a reasonable distance from the radar, so the estimated rain fields are thought to be fairly reliable. CombiPrecip provides discrete measures of rain accumulation that result from post-processing, and this particularity would require specific treatment, for instance using a discrete generalized Pareto distribution (Anderson, 1970; Krishna and Singh Pundir, 2009; Prieto et al., 2014). Here we aim to illustrate the flexibility and advantages of functional peaks-over-threshold analysis, so we leave dealing with the discreteness for future work. To ensure good behaviour of rank-based procedures such as the computation of the empirical extremogram, the original discrete measurements are jittered by adding  $N(0, 10^{-4})$  independent variables.

## 7.2 Risk definition and model formulation

Following de Fondeville and Davison (2018), we model both locally intense and large spatial accumulations of rainfall, but rather than use unnatural risk functions based on standardized data, we here first defined the risk in terms of the jittered measurements  $X_1, \dots, X_n$  through the functionals

$$r_1(X) = |S|^{-1} \int_S X(s) \, ds, \quad r_2(X) = \max_{s \in S} X(s),$$

where  $r_1$  represents a volume of water and thus has a direct hydrological interpretation. In order to use these risk functions to entirely separate these different types of events, we must choose the thresholds  $u_1, u_2 > 0$  so high that only the six most intense events are used for inference; see Figure 1. In order to use more events and to illustrate the flexibility of the functional POT methodology, we study a modified spatial average risk functional,

$$r'_1(X) = |S|^{-1} \int_S X(s) \, ds \times \frac{|\hat{X}_1|}{|\hat{X}|},$$

where  $|\hat{X}|$  denotes the norm of the two-dimensional discrete Fourier transform of  $X$  and  $|\hat{X}_1|$  denotes the norm of its first component. This focuses the risk on events with large spatial average rainfall that are also spatially widespread and discards ‘hybrid’ events: deeper data exploration suggests that more than two types of rain are encountered in this region.

The series  $r'_1(X_i)$  is highly correlated with  $r_1(X_i)$ , especially in the tail, but using the former allows us to lower the threshold enough to retain 36 events. It also illustrates the use of a risk functional that has a non-linear part and shows that image processing ideas can help to characterize extreme rain types; the Appendices extend the theory to nonlinear functionals. Another way to discriminate between types of extremes would be to project the database onto specific weather regimes obtained via EOF analysis (Braud et al., 1993) or via a methodology tailored for extremes (Cooley and Thibaud, 2019), which could help in studying weather patterns such the North American winter dipole (Wang et al., 2015).

When building a model for rainfall, it is important to be able to handle dry grid cells, for

which  $X(s) = 0$ . Below we use a log-Gaussian generalized  $r$ -Pareto process, as presented in Section 3, but this model is defined only for strictly positive functions, so the data must first be transformed to handle zeroes. A simple fix is to construct a new process  $X'$  by adding a positive constant  $c$  to the original data  $X$ , and to treat  $X'(s)$  as left-censored if it equals  $c$ . This implies that the probability of observing rain is the same at each location, which seems reasonable for our region. The value of  $c$  could vary over space to account for inhomogeneities in the distribution of dry cells, for instance by letting  $c(s)$  vary in proportion to the frequency of dry events. Such a modification does not affect the model fit, as  $X' - r(b'_n) = X - r(b_n)$  if the  $b_n$  and  $b'_n$  are chosen to be local empirical quantiles of  $X$  and  $X'$ , though the censoring needs to be accommodated.

To fit the model, we first estimate the marginal tail behaviour and then the dependence model. For the margins we proceed similarly to Section 6.4:  $\hat{b}_n^1$  and  $\hat{b}_n^2$  are defined for  $r_1$  and  $r_2$  separately, as local empirical quantiles of the exceedances for these risk functionals, with the levels chosen such that  $r'_1(b_n^1) = u_1$  and  $r_2(b_n^2) = u_2$ . The corresponding tail indexes and scale parameters are then estimated using the independence likelihood (23).

We considered the Matérn and the Bernstein (Schlather and Moreva, 2017) semi-variogram models for the dependence. In the case of the spatial maximum functional  $r_2$ , we use censored likelihood estimation. For the spatial average functional  $r'_1$ , no dry cells were observed in any of the 36 exceedances, and we can use a gradient score approach to estimate the dependence model. In both cases, we found composite approaches to be more stable, so we estimated the dependence using 1000 random sets of 30 locations for  $r'_1$  and 100 random sets of 10 locations for  $r_2$ , for which the number of subsets was reduced for tractability. We again observed that composite procedures with subsets of size roughly  $n$  gave fairly stable estimates.



### 7.3 Estimated models

The marginal model fit for each risk functional was checked using QQ-plots and was found to be good everywhere. The estimated models, summarized in Figure 12, have two different tail behaviours. Events corresponding to exceedances for  $r'_1$  have estimated tail index  $\hat{\xi}_1 = -0.55_{0.14}$ , and those for  $r_2$  have  $\hat{\xi}_2 = 0.05_{0.04}$ ; the rough standard errors shown as subscripts were obtained by resampling. The estimates suggest that spatially widespread accumulations of rainfall are bounded above, whereas the tail decay for locally heavy rain lies in the Fréchet regime, which gives no upper bound. While one could argue that events for  $r_2$ -exceedances will dominate in the limit, other types of event are nevertheless of interest, especially if we consider more complex definitions of extremes. In this application there appears to be a worst-case scenario for large widespread rainfall over the Sihl river basin that could be used in deriving mitigation procedures, above which we need focus only on locally intense rainfall events.

For  $r'_1$  the lower score was obtained with a Matérn model, while the Bernstein semi-variogram gave a higher likelihood for  $r_2$ -exceedances. The fitted models show much weaker extremal dependence for  $r_2$ , whereas the theoretical extremogram does not drop below 0.7 for  $r_1$ , highlighting the importance of suitable risk definitions. The illustrative simulations in Figure 12 appear consistent with the observations.

The model estimated for  $r_2$  seems to under-estimate extremal dependence compared to the data: we observed that as the threshold increases, the values of the estimated extremogram decreases. This decrease in dependence at high levels is not accommodated by our model, which seems biased toward the most intense (and most localised) events. Huser et al. (2017) and Huser and Wadsworth (2019) have proposed spatial models in which dependence decreases in this way, that could be extended to our setting.

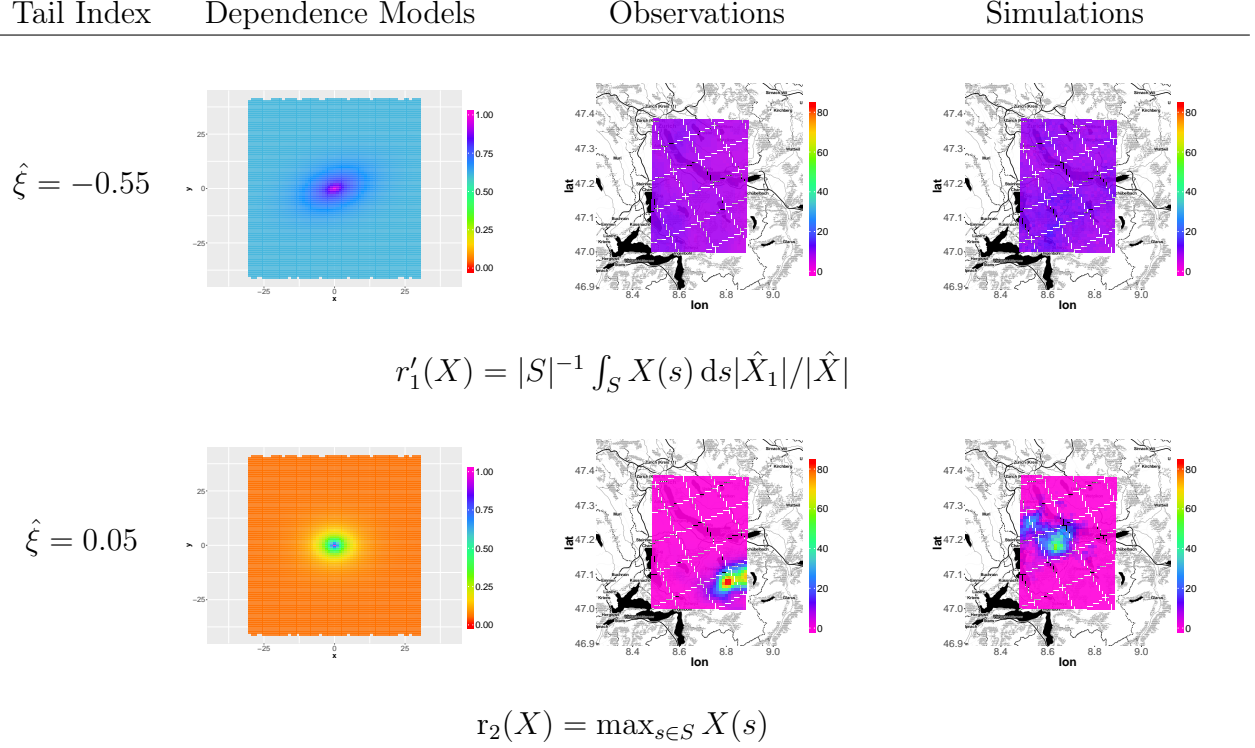


Figure 12: Fitted models for extremes of the modified spatial average (top) and spatial maxima (bottom). Left: estimated tail index and fitted extremogram. Center: largest observed events. Right: simulated events.

## 8 Discussion

Peaks-over-threshold methods are widely used for modelling tails of univariate distributions, but more general procedures are needed to take advantage of complex data. In this paper we extend peaks-over-threshold analysis to extremes of continuous stochastic processes. Exceedances are defined in terms of a real-valued functional  $r$ , and modelled with the generalized  $r$ -Pareto process, which appears as the limit for  $r$ -exceedances of a properly rescaled process and is the functional generalization of the generalized Pareto distribution. We derive construction rules for such processes, give simulation algorithms, highlight their link to max-stable processes, and propose inference and model validation procedures. The ideas are illustrated by applications to extreme windstorms and spatial rainfall.

The minimal assumption to derive the convergence of conditional  $r$ -exceedances, namely a general form of functional regular variation, is quite weak: if the margins are assumed to

have generalized Pareto tails, then the generalized  $r$ -Pareto process arises if one assumes the existence of a non-degenerate joint limit. If this assumption is unrealistic, then the need for a functional model is debatable. The convergence results presented here do not allow asymptotic independence, which would involve limits in which discontinuous functions may appear.

The stochastic windstorm generator obtained in Section 6 produces events consistent with historical records, though the underlying model does not capture the full complexity of the spatio-temporal structure of extreme windstorms, whose dependence changes over space. Oesting et al. (2017) show that the potential types of non-stationarity are limited, but models with varying local anisotropy, such as in Fuglstad et al. (2013) or Fouedjio et al. (2016), would be a natural extension to our work. The realism of simulated storms might be improved by using the methodology of Lindgren et al. (2011) to build physically-inspired non-stationary spatio-temporal dependence structures, using for instance the diffusion equation, and this would be computationally efficient and perhaps more realistic. Our windstorm model introduces non-stationarity by allowing the probability of that a windstorm will occur to depend on explanatory variables, but the distribution of conditional  $r$ -exceedances does not change, and this may be too restrictive. The methodology is flexible enough to incorporate the influence of climate change summaries also on the generalized  $r$ -Pareto process in a similar way.

The rainfall application in Section 7 highlights the importance of an appropriate definition of risk by illustrating how it impacts the tail behaviour of the selected events and showing how the notion of  $r$ -exceedance allows one to disentangle mixtures of extremes. Also sub-asymptotic models for which extremal dependence diminishes with intensity are required, as this phenomenon is commonly observed.

Another notion of complexity for extremes is linked with compound events. Let  $X = (X^1, X^2)$  be a bivariate continuous stochastic process and let  $r^1$  and  $r^2$  be suitable risk

functionals. Then under conditions similar to those in the paper, the functional

$$r(X^1, X^2) = \min \{r^1(X^1) - u^1, r^2(X^2) - u^2\}$$

can be used to characterize extremes of both types and could be applied when studying infrastructure that is vulnerable to different sources of risk.

## Acknowledgement

We thank the Swiss National Science Foundation for financial support. Alexis Berne and Gionata Ghiggi kindly gave us access to the Swiss radar rainfall data, which were originally provided by Meteoswiss.

## References

- Anderson, C. W. (1970). Extreme Value Theory for a Class of Discrete Distributions with Applications to Some Stochastic Processes. *Journal of Applied Probability*, 7(1):99–113.
- Asadi, P., Davison, A. C., and Engelke, S. (2015). Extremes on River Networks. *Annals of Applied Statistics*, 9(4):2023–2050.
- Balkema, A. A. and de Haan, L. (1974). Residual life time at great age. *Annals of Probability*, 2(792–804).
- Beirlant, J., Goegebeur, Y., Segers, J., and Teugels, J. (2004). *Statistics of Extremes: Theory and Applications*. Wiley, Chichester.
- Bezzola, G. and Hegg, C. (2007). Ereignisanalyse Hochwasser 2005, Teil 1 - Prozesse, Schäden und erste Einordnung. Technical report.
- Blessing, S., Fraedrich, K., Junge, M., Kunz, T., and Lunkeit, F. (2005). Daily North-

- Atlantic Oscillation (NAO) index: Statistics and its Stratospheric Polar Vortex Dependence. *Meteorologische Zeitschrift*, 14(6):763–769.
- Braud, I., Obled, C., and Phamdinhtuan, A. (1993). Empirical Orthogonal Function (EOF) Analysis of Spatial Random Fields: Theory, Accuracy of the Numerical Approximations and Sampling Effects. *Stochastic Hydrology and Hydraulics*, 7(2):146–160.
- Brown, B. M. and Resnick, S. I. (1977). Extreme Values of Independent Stochastic Processes. *Journal of Applied Probability*, 14(4):732–739.
- Castruccio, S., Huser, R., and Genton, M. G. (2016). High-Order Composite Likelihood Inference for Max-Stable Distributions and Processes. *Journal of Computational and Graphical Statistics*, 25(4):1212–1229.
- Cloke, H. L. and Pappenberger, F. (2009). Ensemble Flood forecasting: A Review. *Journal of Hydrology*, 375(3-4):613–626.
- Coles, S. G. and Tawn, J. A. (1991). Modelling Extreme Multivariate Events. *Journal of the Royal Statistical Society. Series B (Methodological)*, 53(2):377–392.
- Coles, S. G. and Tawn, J. A. (1994). Statistical Methods for Multivariate to Structural Design Extremes: an Application to Structural Design. *Journal of the Royal Statistical Society. Series C (Applied Statistics)*, 43(1):1–48.
- Coles, S. G. and Tawn, J. A. (1996). Modelling Extremes of the Areal Rainfall Process. *Journal of the Royal Statistical Society. Series B (Methodological)*, 58(2):329–347.
- Cooley, D., Naveau, P., and Poncet, P. (2006). Variograms for max-stable random fields. In Bertail, P., Doukhan, P., and Soulier, P., editors, *Dependence in Probability and Statistics*, volume 187 of *Lecture Notes in Statistics*, pages 373–390. Springer, New York.
- Cooley, D. and Thibaud, E. (2019). Decompositions of Dependence for High-dimensional Extremes. *Biometrika*, 106(3):1–18.

- Davis, R. A. and Mikosch, T. (2009). The Extremogram: a Correlogram for Extreme Events. *Bernoulli*, 15(4):977–1009.
- Davis, R. A., Mikosch, T., and Zhao, Y. (2013). Measures of serial extremal dependence and their estimation. *Stochastic Processes and their Applications*, 123(7):2575–2602.
- Davison, A. C. (1984). Modelling excesses over high thresholds, with an application. In de Oliveira, J. T., editor, *Statistical Extremes and Applications*, pages 461–482. Reidel, Dordrecht.
- Davison, A. C. and Gholamrezaee, M. M. (2012). Geostatistics of Extremes. *Proceedings of the Royal Society A: Mathematical, Physical and Engineering Sciences*, 468(2138):581–608.
- Davison, A. C. and Smith, R. L. (1990). Models for Exceedances over High Thresholds (with discussion). *Journal of the Royal Statistical Society. Series B (Methodological)*, 52(3):393–442.
- Dawid, P. A., Musio, M., and Ventura, L. (2016). Minimum Scoring Rule Inference. *Scandinavian Journal of Statistics*, 43(1):123–138.
- de Fondeville, R. (2016). mvPot — R package version 0.1.1.
- de Fondeville, R. and Davison, A. C. (2018). High-dimensional Peaks-over-threshold Inference. *Biometrika*, 105(3):575–592.
- de Haan, L. (1984). A Spectral Representation for Max-stable Processes. *The Annals of Probability*, 12(4):1194–1204.
- de Haan, L. and Ferreira, A. (2006). *Extreme Value Theory: An Introduction*. Springer, New York, USA.
- Dee, D. P., Uppala, S. M., Simmons, A. J., Berrisford, P., Poli, P., Kobayashi, S., Andrae, U., Balmaseda, M. A., Balsamo, G., Bauer, P., Bechtold, P., Beljaars, A. C. M., van de

- Berg, L., Bidlot, J., Bormann, N., Delsol, C., Dragani, R., Fuentes, M., Geer, A. J., Haimberger, L., Healy, S. B., Hersbach, H., Hólm, E. V., Isaksen, L., Kållberg, P., Köhler, M., Matricardi, M., McNally, A. P., Monge-Sanz, B. M., Morcrette, J.-J., Park, B.-K., Peubey, C., de Rosnay, P., Tavolato, C., Thépaut, J.-N., and Vitart, F. (2011). The ERA-Interim reanalysis: configuration and performance of the data assimilation system. *Quarterly Journal of the Royal Meteorological Society*, 137(656):553–597.
- Della Marta, P. and Mathis, H. (2008). The return period of wind storms over Europe. *International Journal of Climatology*, 29(3):437–459.
- Della-Marta, P. M., Liniger, M. A., Appenzeller, C., Bresch, D. N., Köllner-Heck, P., and Muccione, V. (2010). Improved estimates of the European winter windstorm climate and the risk of reinsurance loss using climate model data. *Journal of Applied Meteorology and Climatology*, 49(10):2092–2120.
- Dombry, C., Engelke, S., and Oesting, M. (2016). Exact Simulation of Max-stable Processes. *Biometrika*, 103(2):303–317.
- Dombry, C. and Ribatet, M. (2015). Functional Regular Variations, Pareto Processes and Peaks Over Thresholds. *Statistics and Its Interface*, 8(1):9–17.
- Donat, M., Leckebusch, G., Pinto, J., and Ulbrich, U. (2010). European Storminess and Associated Circulation Weather Types: Future Changes Deduced from a Multi-model Ensemble of GCM Simulations. *Climate Research*, 42(1):27–43.
- Donat, M. G., Leckebusch, G. C., Wild, S., and Ulbrich, U. (2011). Future Changes in European Winter Storm Losses and Extreme Wind Speeds Inferred from GCM and RCM Multi-model Simulations. *Natural Hazards and Earth System Science*, 11(5):1351–1370.
- Economou, T. and David, B. (2014). Spatio-temporal Modelling of Extreme Storms. *Annals of Applied Statistics*, 8(4):2223–2246.

- Einmahl, J. H. J., Kiriliouk, A., Krajina, A., and Segers, J. (2016a). An M-estimator of Spatial Tail Dependence. *Journal of the Royal Statistical Society. Series B (Statistical Methodology)*, 78(1):275–298.
- Einmahl, J. H. J., Kiriliouk, A., and Segers, J. (2016b). A Continuous Updating Weighted Least Squares Estimator of Tail Dependence in High Dimensions. *Journal of Statistical Planning and Inference*, 169(12):22–33.
- Embrechts, P., Klüppelberg, C., and Mikosch, T. (1997). *Modelling Extremal Events for Insurance and Finance*. Springer-Verlag, Berlin.
- Engelke, S., de Fondeville, R., and Oesting, M. (2019). Extremal Behaviour of Aggregated Data with an Application to Downscaling. *Biometrika*, 106(1):127–144.
- Engelke, S. and Malinowski, A. (2014). Statistical Inference for Max-stable Processes by Conditioning on Extreme Events. *Advances in Applied Probability*, 46(2):478–495.
- Engelke, S., Malinowski, A., Kabluchko, Z., and Schlather, M. (2015). Estimation of Hüsler–Reiss Distributions and Brown–Resnick Processes. *Journal of the Royal Statistical Society. Series B (Statistical Methodology)*, 77(1):239–265.
- Ferreira, A. and de Haan, L. (2014). The Generalized Pareto Process; with a View Towards Application and Simulation. *Bernoulli*, 20(4):1717–1737.
- Ferreira, A., de Haan, L., and Zhou, C. (2012). Exceedance Probability of the Integral of a Stochastic Process. *Journal of Multivariate Analysis*, 105(1):241–257.
- Fisher, R. A. and Tippett, L. H. C. (1928). Limiting Forms of the Frequency Fistribution of the Largest or Smallest Member of a Sample. *Mathematical Proceedings of the Cambridge Philosophical Society*, 24(2):180–190.
- Fouedjio, F., Desassis, N., and Rivoirard, J. (2016). A generalized Convolution Model and Estimation for Non-stationary Random Functions. *Spatial Statistics*, 16(1):35–52.



- Fuglstad, G.-A., Lindgren, F., Simpson, D., and Rue, H. (2013). Exploring a New Class of Non-stationary Spatial Gaussian Random Fields with Varying Local Anisotropy.
- Fuglstad, G.-A., Lindgren, F., Simpson, D., and Rue, H. (2015). Exploring a New Class of Non-stationary Spatial Gaussian Random Fields with Varying Local Anisotropy. *Statistica Sinica*, 25(1):115–133.
- Gabella, M., Speirs, P., Hamann, U., Germann, U., and Berne, A. (2017). Measurement of Precipitation in the Alps Using Dual-polarization C-Band Ground-based Radars, the GPM Spaceborne Ku-Band Radar, and Rain Gauges. *Remote Sensing*, 9(11):1147–1166.
- Gelfand, A. E., Diggle, P. J., Fuentes, M., and Guttorp, P. (2010). *Handbook of Spatial Statistics*. Chapman & Hall/CRC Press, New York, USA.
- Gnedenko, B. (1943). Sur la Distribution Limite du Terme Maximum d’une Série Aléatoire. *Annals of Mathematics*, 44(3):423–453.
- Gneiting, T. and Raftery, A. E. (2007). Strictly Proper Scoring Rules, Prediction, and Estimation. *Journal of the American Statistical Association*, 102(477):359–378.
- Hall, T. M. and Jewson, S. (2008). Comparison of local and basinwide methods for risk assessment of tropical cyclone landfall. *Journal of Applied Meteorology and Climatology*, 47(2):361–367.
- Haylock, M. (2011). European Extra-tropical Storm Damage Risk from a Multi-model Ensemble of Dynamically-downscaled Global Climate Models. *Natural Hazards and Earth System Science*, 11(10):2847–2857.
- Hosking, J. R. M. and Wallis, J. R. (1987). Parameter and Quantile Estimation for Generalized Pareto Distribution. *Technometrics*, 29(3):339–349.
- Hult, H. and Lindskog, F. (2005). Extremal Behavior of Regularly Varying Stochastic Processes. *Stochastic Processes and their Applications*, 115(2):249–274.

- Huser, R. and Davison, A. C. (2013). Composite Likelihood Estimation for the Brown–Resnick Process. *Biometrika*, 100(2):511–518.
- Huser, R., Davison, A. C., and Genton, M. G. (2016). Likelihood Estimators for Multivariate Extremes. *Extremes*, 19(1):79–103.
- Huser, R., Opitz, T., and Thibaud, E. (2017). Bridging Asymptotic Independence and Dependence in Spatial Extremes Using Gaussian Scale Mixtures. *Spatial Statistics*, 21(1):166–186.
- Huser, R. and Wadsworth, J. L. (2019). Modeling Spatial Processes with Unknown Extremal Dependence Class. *Journal of the American Statistical Association*, 114(525):434–444.
- Jaun, S., Ahrens, B., Walser, A., Ewen, T., and Schär, C. (2008). A Probabilistic View on the August 2005 Floods in the Upper Rhine Catchment. *Natural Hazards and Earth System Sciences*, 8(1):281–291.
- Katz, R. W., Parlange, M. B., and Naveau, P. (2002). Statistics of Extremes in Climatology. *Advances in Water Resources*, 25(8-12):1287–1304.
- Klüppelberg, C. and Resnick, S. I. (2008). The Pareto Copula, Aggregation of Risks, and the Emperor’s Socks. *Journal of Applied Probability*, 45(1):67–84.
- Krishna, H. and Singh Pundir, P. (2009). Discrete Burr and Discrete Pareto Distributions. *Statistical Methodology*, 6(2):177–188.
- Ledford, A. W. and Tawn, J. A. (1996). Statistics for Near Independence in Multivariate Extreme Values. *Biometrika*, 83(1):169–187.
- Lindgren, F., Rue, H., and Lindström, J. (2011). An Explicit Link Between Gaussian Fields and Gaussian Markov Random Fields: the Stochastic Partial Differential Equation Approach (with discussion). *Journal of the Royal Statistical Society. Series B (Statistical Methodology)*, 73(4):423–498.

- Lindskog, F., Resnick, S. I., and Roy, J. (2014). Regularly Varying Measures on Metric Spaces: Hidden Regular Variation and Hidden Jumps. *Probability Surveys*, 11(1):270–314.
- Matern, B. (1960). *Spatial Variation*. Springer, New York.
- NERC (1975). *The Flood Studies Report*. The Natural Environment Research Council, London.
- Oesting, M., Schlather, M., and Friederichs, P. (2017). Statistical Post-Processing of Forecasts for Extremes Using Bivariate Brown-Resnick Processes with an Application to Wind Gusts. *Extremes*, 20(2):309–332.
- Opitz, T. (2013a). Extremal  $\mathbb{S}^d$ -processes: Elliptical Domain of Attraction and a Spectral Representation. *Journal of Multivariate Analysis*, 122(1):409–413.
- Opitz, T. (2013b). *Extrêmes Multivariés et Spatiaux : Approches Spectrales et Modèles Elliptiques*. PhD thesis, Université Montpellier II.
- Padoan, S. A., Ribatet, M., and Sisson, S. A. (2010). Likelihood-Based Inference for Max-Stable Processes. *Journal of the American Statistical Association*, 105(489):263–277.
- Panziera, L., Gabella, M., Germann, U., and Martius, O. (2018). A 12-year Radar-based Climatology of Daily and Sub-daily Extreme Precipitation over the Swiss Alps. *International Journal of Climatology*, 38(10):3749–3769.
- Pfahl, S. (2014). Characterising the Relationship Between Weather Extremes in Europe and Synoptic Circulation Features. *Natural Hazards and Earth System Science*, 14(6):1461–1475.
- Pickands, J. (1975). Statistical inference using extreme order statistics. *Annals of Statistics*, 3:119–131.

- Pinto, J., Karremann, M., Born, K., Della-Marta, P., and Klawe, M. (2012). Loss Potentials Associated with European Windstorms under Future Climate Conditions. *Climate Research*, 54(1):1–20.
- Powell, M. D. and Reinhold, T. A. (2007). Tropical Cyclone Destructive Potential by Integrated Kinetic Energy. *Bulletin of the American Meteorological Society*, 88(1):513–526.
- Prieto, F., Gómez-Déniz, E., and Sarabia, J. M. (2014). Modelling Road Accident Blackspots Data with the Discrete Generalized Pareto Distribution. *Accident Analysis and Prevention*, 71(1):38–49.
- Resnick, S. I. (1987). *Extreme Values, Regular Variation, and Point Processes*. Springer-Verlag, New York, USA.
- Roberts, J. F., Champion, A. J., Dawkins, L. C., Hodges, K. I., Shaffrey, L. C., Stephenson, D. B., Stringer, M. A., Thornton, H. E., and Youngman, B. D. (2014). The XWS Open Access Catalogue of Extreme European Windstorms from 1979 to 2012. *Natural Hazards and Earth System Sciences*, 14(9):2487–2501.
- Rootzén, H., Segers, J., and Wadsworth, J. L. (2018a). Multivariate Generalized Pareto Distributions: Parametrizations, Representations, and Properties. *Journal of Multivariate Analysis*, 165(1):117–131.
- Rootzén, H., Segers, J., and Wadsworth, J. L. (2018b). Multivariate Peaks-over-thresholds Models. *Extremes*, 21(1):115–145.
- Rootzén, H. and Tajvidi, N. (2006). Multivariate Generalized Pareto Distributions. *Bernoulli*, 12(5):917–930.
- Schlather, M. and Moreva, O. (2017). A Parametric Model Bridging Between Bounded and Unbounded Variograms. *Stat*, 6(1):47–52.

- Sharkey, P., Tawn, J. A., and Brown, S. J. (2020). Modelling the spatial extent and severity of extreme European windstorms. *Applied Statistics*, page to appear.
- Sideris, I. V., Gabella, M., Erdin, R., and Germann, U. (2014). Real-time Radar-rain-gauge Merging Using Spatio-temporal Co-kriging with External Drift in the Alpine Terrain of Switzerland. *Quarterly Journal of the Royal Meteorological Society*, 140(680):1097–1111.
- Smith, R. L. (1984). Threshold methods for sample extremes. In de Oliveira, J. T., editor, *Statistical Extremes and Applications*, pages 621–638. Reidel, Dordrecht.
- Smith, R. L. (1990). Max-stable processes and spatial extremes. Technical report.
- Thibaud, E. and Opitz, T. (2015). Efficient Inference and Simulation for Elliptical Pareto Processes. *Biometrika*, 102(4):855–870.
- Todorovic, P. and Rousselle, J. (1971). Some problems of flood analysis. *Water Resources Research*, 7:1144–1150.
- Todorovic, P. and Zelenhasic, E. (1970). A stochastic model for flood analysis. *Water Resources Research*, 6:1641–1648.
- Vautard, R., van Oldenborgh, G. J., Otto, F. E. L., Yiou, P., de Vries, H., van Meijgaard, E., Stepek, A., Soubeyroux, J.-M., Philip, S., Kew, S. F., Costella, C., Singh, R., and Tebaldi, C. (2019). Human Influence on European Winter Wind Wtorms such as those of January 2018. *Earth System Dynamics*, 10(2):271–286.
- Wadsworth, J. L. and Tawn, J. A. (2014). Efficient Inference for Spatial Extreme Value Processes Associated to Log-Gaussian Random Functions. *Biometrika*, 101(1):1–15.
- Wang, S. Y. S., Huang, W. R., and Yoon, J. H. (2015). The North American Winter ‘Dipole’ and Extremes Activity: A CMIP5 Assessment. *Atmospheric Science Letters*, 16(3):338–345.

- Weller, G. B., Cooley, D., Sain, S. R., Bukovsky, M. S., and Mearns, L. O. (2013). Two Case Ctudies on NARCCAP Precipitation Extremes. *Journal of Geophysical Research Atmospheres*, 118(18):10475–10489.
- Whittle, P. (1954). On Stationary Processes in the Plane. *Biometrika*, 41(3):434–449.
- Whittle, P. (1963). Stochastic Processes in Several Dimensions. *Bulletin of the International Statistical Institute*, 40(2):974–994.
- Yiou, P. (2014). AnaWEGE: a weather generator based on analogues of atmospheric circulation. *Geoscientific Model Development*, 7(2):531–543.

## A Limit tail distribution for non-linear risk functionals

In this appendix we derive the limiting distributions of  $r$ -exceedances under minimal assumptions on the risk functional. A risk functional  $r : \mathcal{F} \rightarrow \mathbb{R}$  is said to be valid for the process  $X \in \text{GRV}(\xi, a_n, b_n, \Lambda)$  if there exists a positive continuous real-valued function  $A$  such that

$$\lim_{n \rightarrow \infty} \sup_{s \in S} \left| \frac{a_n(s)}{r(a_n)} - A(s) \right| = 0, \quad (27)$$

and if

$$\begin{aligned} r \text{ is continuous at } -\xi^{-1}A, \quad r(-A\xi^{-1}) < 0, \quad \xi > 0, \\ r(x) \rightarrow -\infty \quad \text{as } x \rightarrow -\infty, \quad \xi \leq 0. \end{aligned} \quad (28)$$

Equations (27) and (28) give the minimal properties of the functional  $r$  needed in order to describe the limiting distribution of  $r$ -exceedances of  $(X - b_n)/r(a_n)$  over a threshold  $u \geq 0$ .

Similarly to the linear case, condition (27) implies that  $a_n(s) \approx r(a_n)A(s)$  for large  $n$ , but it also implies that the convergence rates of  $r(a_n)$  and  $a_n(s)$  must be the same for all  $s \in S$ . For instance, when  $\xi > 0$ , the class of 1-homogeneous functionals satisfies (27) and (28).

THEOREM 2. *Let  $X$  be a stochastic process whose sample paths lie in  $C(S)$ . If  $X \in \text{GRV}(\xi, a_n, b_n, \Lambda)$  and  $r$  is a valid risk functional for  $X$ , then*

$$\Pr \left[ \left\lfloor \frac{X - b_n}{r(a_n)} \right\rfloor \in (\cdot) \mid r \left\{ \frac{X - b_n}{r(a_n)} \right\} \geq u \right] \rightarrow \Pr \{P \in (\cdot)\}, \quad n \rightarrow \infty, \quad (29)$$

where  $u \geq 0$  and  $P$  is a generalized  $r$ -Pareto process with tail index  $\xi$ , scale  $A$ , zero location and measure  $\Lambda$ . When  $\xi > 0$ , we write  $\lfloor \cdot \rfloor = \max\{(\cdot), -\xi A\}$  with the maxima taken componentwise, and when  $\xi \leq 0$  we take  $\lfloor \cdot \rfloor$  to be the identity operator.

Theorem 2 implies that the generalized  $r$ -Pareto process is the only possible limit for  $r$ -exceedances of properly rescaled regularly-varying stochastic processes. Hence, for any  $X \in \text{GRV}(\xi, a_n, b_n, \Lambda)$  and sufficiently large  $n$ , the distribution of  $r$ -exceedances of the process  $(X - b_n)/r(a_n)$  over a threshold  $u \geq 0$  can be approximated by a generalized  $r$ -Pareto process  $P$ . The linear transformation required in Theorem 2 before characterizing the risk is both simpler and closer to the original data than classical marginal transforms (Kluppelberg and Resnick, 2008), as it does not modify the tail decay regime. For the class of homogeneous functionals and  $\xi > 0$ , we can choose  $b_n = 0$ , and then Theorem 2 retrieves the work of Dombry and Ribatet (2015), which describes the limiting distribution of  $X - b_n$  for increasingly high thresholding of  $r(X - b_n)$ . Assumption (27) could be relaxed by replacing  $(X - b_n)/r(a_n)$  by  $X - b_n/a_n$  in the previous results.

## A.1 Generalized $r$ -Pareto processes: definition and properties

We now describe the family of generalized  $r$ -Pareto process when the functional satisfies only conditions (27) and (28). Consider the set of positive functions

$$\mathcal{A}_r = \begin{cases} \left\{ y \in \mathcal{F}_+ : r \left( A \frac{y^\xi - 1}{\xi} \right) \geq 0 \right\}, & \xi \neq 0, \\ \{ y \in \mathcal{F}_+ : r(A \log y) \geq 0 \}, & \xi = 0. \end{cases}$$

DEFINITION 2. Let  $a > 0$  and  $b$  be continuous functions on  $S$ , let  $r : \mathcal{F} \rightarrow \mathbb{R}$  be a valid risk functional, let  $\Lambda$  be a  $(-1)$ -homogeneous measure on  $\mathcal{F}_+$  and define  $A = a/r(a)$ . The generalized  $r$ -Pareto process  $P$  associated to the measure  $\Lambda$  and tail index  $\xi \in \mathbb{R}$  is the stochastic process on  $\{x \in \mathcal{F}^{\xi, a, b} : r\{(x - b)/r(a)\} \geq 0\}$  defined as

$$P = \begin{cases} a(Y_r^\xi - 1)/\xi + b, & \xi \neq 0, \\ a \log Y_r + b, & \xi = 0, \end{cases} \quad (30)$$

where  $Y_r$  is the stochastic process on  $\mathcal{A}_r$  with probability measure  $\Lambda(\cdot)/\Lambda\{\mathcal{A}_r\}$ .

Similarly to the linear case, the conditional marginal distributions of the generalized  $r$ -Pareto process are also univariate generalized Pareto, but there is no simple expression for the distribution of  $r\{(P - b)/r(a)\}$ , which can only be evaluated by simulation.

The process  $P$  of Definition 2 is closely related to the stochastic process  $Y_r$  defined on  $\mathcal{A}_r$  with probability measure  $\Lambda(\cdot)/\Lambda\{\mathcal{A}_r\}$ . The pseudo-polar representation (12) of  $Y_r$  is key to deriving algorithms for the simulation of generalized  $r$ -Pareto processes.

## A.2 Simulation algorithm

Let  $r$  be a valid risk functional and let  $P$  be the corresponding generalized  $r$ -Pareto process with measure  $\Lambda$ , tail index  $\xi \in \mathbb{R}$ , scale function  $a > 0$  and location function  $b$ . We suppose that we have a threshold  $u \geq 0$ , which is deterministic and can be found analytically, such that

$$\mathcal{A}_r \subset \{y \in \mathcal{F}_+ : \|y\|_1 \geq u\}. \quad (31)$$

Algorithm 2 enables simulation of  $P$  when an algorithm for  $Y_r$  is available. Its efficiency is determined by the capacity to find the largest possible  $u$ ,  $u_{\sup}$ , say, such that (31) is satisfied, and its rejection rate is the ratio of the measures of the sets  $\mathcal{A}_r$  and  $\{y \in \mathcal{F}_+ : \|y\|_1 \geq u\}$ .



---

**Algorithm 2:** Simulation of generalized  $r$ -Pareto process,  $P$ 


---

```

Set  $Y_r = 0$ ;
while  $r[A\xi^{-1}\{(Y_r)^\xi - 1\}] < 0$  do
    generate a unit Pareto random variable  $R$ ;
    generate  $W_1$  on  $\mathcal{S}_{\|\cdot\|_1} = \{y \in \mathcal{F}_+ : \|y\|_1 = 1\}$  with probability measure  $\sigma_0$  in (13);
    set  $Y_r = RW_1/u$ ;
end
Set  $P = a\xi^{-1}\{(Y_r)^\xi - 1\} + b$ ;

```

---

### A.3 Link to max-stable processes

As in the linear case, the Poisson process representation of max-stable processes (de Haan, 1984) links them to generalized  $r$ -Pareto processes. We consider the Poisson process  $(R_j, W_j)_{j=1, \dots}$  on  $(0, \infty) \times \mathcal{S}_0$  with intensity measure  $r^{-2}dr \times \sigma_0(dw)$ , where  $\sigma_0$  is given by (13). Then the process

$$M(s) = \begin{cases} \sup_{j \geq 1} a(s) \frac{\{R_j W_j(s)\}^\xi - 1}{\xi} + b(s), & \xi \neq 0, \\ \sup_{j \geq 1} a(s) \log\{R_j W_j(s)\} + b(s), & \xi = 0, \end{cases} \quad s \in S, \quad (32)$$

is max-stable with exponent measure  $\Lambda \circ T_{\xi, a, b}(\cdot)$  (Resnick, 1987, Proposition 3.7), where  $T_{\xi, a, b}(z)$  is the non-atomic map

$$T_{\xi, A, B}(z) = \begin{cases} \{1 + \xi(z - b)/a\}_+^{1/\xi}, & \xi \neq 0, \\ \exp\{(z - b)/a\}, & \xi = 0. \end{cases}$$

With this notation, the finite-dimensional distribution of  $M$  at locations  $s_1, \dots, s_L \in S$  is again (16).

### A.4 Statistical inference

Statistical inference for generalized  $r$ -Pareto processes with non-linear risk functional follows the same principle as in Section 4 and relies on the approximation

$$\Pr\left\{\frac{X - b_n}{r(a_n)} \in \mathcal{A}\right\} \approx \Pr\left(1 \left[r \left\{\frac{X - b_n}{r(a_n)}\right\} \geq 0\right] = 1\right) \times \Pr(P \in \mathcal{A}), \quad (33)$$

where  $\mathcal{A} \subset \mathcal{A}(0) = \{x \in \mathcal{F}^{\xi, A, 0} : r(x) \geq 0\}$  for sufficiently large  $n$ . Likelihood-based inference using (33) is delicate in general. Indeed, estimating the marginal parameters jointly with the dependence parameters is unlikely to be numerically stable if the set of observed  $r$ -exceedances,  $\{x_j : r\{(x_j - b_n)/r(a_n)\} \geq 0, j = 1, \dots, n\}$ , depends on  $a_n$  and  $b_n$ . Thus it is necessary to either restrict the choice of functional to those for which  $\mathcal{E}_r$  is independent of the rescaling, as is the case for linear functionals, or to use a two-step procedure. In the latter, we first estimate the marginal parameters  $\hat{a}_n$ ,  $\hat{b}_n$  and  $\hat{\xi}$  and then fix them while estimating the dependence model. To have a marginal model tailored to the  $r$ -exceedances and to thus disentangle any mixtures present in the tail, we propose an iterative procedure. The underlying principle is, if necessary, to refine a different risk functional  $r'$  until the set of  $r'$ -exceedances of  $(x_j - \hat{b}_n)/r(\hat{a}_n)$  equals the set of  $r$ -exceedances of  $r(x_j)$ ,  $j = 1, \dots, n$ . To do so, we

1. set  $a = 1$ ,  $b = 0$ , and  $\mathcal{E}_r = \{x_j : r(x_j) \geq 0, j = 1, \dots, n\}$ ;
2. define or refine  $r'$ ;
3. fit marginal parameters using the set of observations  $\mathcal{E}_{r'} = \{x_j : r'\{(x_j - \hat{b}_n)/r(\hat{a}_n)\} \geq 0, j = 1, \dots, n\}$ ;
4. set  $a = \hat{a}_n$  and  $b = \hat{b}_n$ ;
5. return to step 2 if  $\mathcal{E}_{r'} \neq \mathcal{E}_r$ .

An example of functional refinement inspired by the application of Section 7 consists of modifying the frequency domain of a Fourier filter until  $\mathcal{E}_r$  and  $\mathcal{E}_{r'}$  are equal.

Identifiability issues caused by the conditional nature of generalized  $r$ -Pareto processes might also arise. A natural idea is to set  $b_n$  equal to local empirical quantiles estimated from  $\mathcal{E}_r$ . Apart from these considerations, the inference procedures described in Section 4 can be used in the same way.

## B Proofs

### B.1 Theorem 2

Recall that  $S \subset \mathbb{R}^D$  ( $D \geq 1$ ) is a compact metric space, that  $\mathcal{F}$  denotes the Banach space of real-valued continuous functions on  $S$  with norm  $\|x\|$  and that  $\mathcal{F}_+$  denotes the subset of  $\mathcal{F}$  containing only non-negative functions that are not everywhere zero; thus  $\mathcal{F}_+$  excludes the zero function. When studying extremes the cones  $\{0\}$  or  $\{x \in \mathcal{F}_+ : \inf_{s \in S} x(s) = 0\}$  are often excluded from the set of continuous non-negative functions over  $S$  to avoid the appearance of points with infinite mass in the limiting measure. Let  $M_{\mathcal{F}_+}$  denote the class of Borel measures on the Borel sigma-algebra  $\mathcal{B}(\mathcal{F}_+)$  associated to  $\mathcal{F}_+$ . We say that a set  $\mathcal{A} \in \mathcal{B}(\mathcal{F}_+)$  is bounded away from the zero function  $\{0\}$  if  $d(\mathcal{A}, \{0\}) = \inf_{x \in \mathcal{A}} \|x\| > 0$ .

A sequence of measures  $\{\Lambda_n\} \subset M_{\mathcal{F}_+}$  is said to converge to a limit  $\Lambda \in M_{\mathcal{F}_+}$ , written  $\Lambda_n \xrightarrow{\hat{w}} \Lambda$  (Hult and Lindskog, 2005), if  $\lim_{n \rightarrow \infty} \Lambda_n(\mathcal{A}) = \Lambda(\mathcal{A})$ , for all  $\mathcal{A} \in \mathcal{B}(\mathcal{F}_+)$  bounded away from  $\{0\}$  with  $\Lambda(\partial\mathcal{A}) = 0$ , where  $\partial\mathcal{A}$  denotes the boundary of  $\mathcal{A}$ . For equivalent definitions of this  $\hat{w}$ -convergence, so-called, see Lindskog et al. (2014, Theorem 2.1). If  $r$  is a 1-homogeneous functional then the set  $\mathcal{C}_r = \{x \in \mathcal{F}_+ : r(x) = 0\}$  is a cone of  $\mathcal{F}_+$ , so Theorem 2.3 of Lindskog et al. (2014) implies that any measure regularly varying on  $\mathcal{F}_+$  is also regularly varying on  $\mathcal{F}_+$  from which a cone is excluded.

We proceed similarly as in Engelke et al. (2019). Let  $X \in \text{GRV}(\xi, a_n, b_n, \Lambda)$  be as defined in Section 2.3 and suppose first that  $\xi > 0$ . The continuous function  $A$  is strictly positive and thus bounded away from zero on the compact set  $S$ . Hence, for any  $\varepsilon > 0$ , equation (27) gives  $|r(a_n)^{-1}a_n(s) - A(s)| < \varepsilon A(s)$  for all  $s \in S$  and sufficiently large  $n$ . If so, for  $\xi \neq 0$ ,

$$\frac{X - b_n}{r(a_n)} = \frac{a_n}{r(a_n)} \frac{X - b_n}{a_n} \geq (1 - \varepsilon)A\left(\frac{X - b_n}{a_n}\right) - \varepsilon,$$

and likewise

$$\frac{X - b_n}{r(a_n)} \leq (1 + \varepsilon)A \left( \frac{X - b_n}{a_n} \right) + \varepsilon.$$

With  $\varepsilon \rightarrow 0$ , equation (4) leads to

$$\lim_{n \rightarrow \infty} n \Pr \left\{ \left\lfloor \frac{X - b_n}{r(a_n)} \right\rfloor \in (\cdot) \right\} = \lim_{n \rightarrow \infty} n \Pr \left\{ A \left\lfloor \frac{X - b_n}{a_n} \right\rfloor \in (\cdot) \right\} = \Lambda \left\{ y \in \mathcal{F}_+ : A \frac{y^\xi - 1}{\xi} \in (\cdot) \right\}.$$

For  $\xi > 0$ , by assumption  $r(-A\xi^{-1}) < 0$ , and  $r$  is continuous at  $-A\xi^{-1}$ , ensuring that

$$d_\infty \left[ \left\{ y \in \mathcal{F}_+ : r \left( A \frac{y^\xi - 1}{\xi} \right) \geq 0 \right\}, \{0\} \right] > 0,$$

so the set  $\left\{ y \in \mathcal{F}_+ : r \left( A \frac{y^\xi - 1}{\xi} \right) \geq 0 \right\}$  is bounded away from the singleton  $\{0\}$ . Thus we can apply  $\hat{w}$ -convergence on any set  $\mathcal{A} \subset \left\{ y \in \mathcal{F}_+ : r \left( A \frac{y^\xi - 1}{\xi} \right) \geq 0 \right\}$ , yielding

$$\lim_{n \rightarrow \infty} \Pr \left[ \left\lfloor \frac{X - b_n}{r(a_n)} \right\rfloor \in \mathcal{A} \mid r \left\{ \frac{X - b_n}{r(a_n)} \right\} \geq 0 \right] = \frac{\Lambda(\mathcal{A})}{\Lambda \left\{ y \in \mathcal{F}_+ : r \left( A \frac{y^\xi - 1}{\xi} \right) \geq 0 \right\}}.$$

For  $\xi \leq 0$ , the hypothesis  $r(x) \rightarrow -\infty$  as  $x \rightarrow -\infty$  ensures that  $\{y \in \mathcal{F}_+ : r(A \log y) \geq 0\}$  and  $\{y \in \mathcal{F}_+ : r\{A\xi^{-1}(y^\xi - 1)\} \geq 0\}$  are also bounded away from  $\{0\}$ . The case  $\xi < 0$  is analogous to the Fréchet domain of attraction and for  $\xi = 0$  we use

$$\lim_{n \rightarrow \infty} n \Pr \left[ \frac{X - b_n}{r(a_n)} \in \mathcal{A} \right] = \Lambda \{y \in \mathcal{F}_+ : (A \log y + B) \in \mathcal{A}\},$$

which proves the theorem. □

## B.2 Theorem 1

We start with the conclusion of Theorem 2. For  $\xi \neq 0$ , we use the pseudo-polar decomposition centered at  $-\xi^{-1}A$ , i.e.,

$$\rho = r(x) + \xi^{-1}, \quad w = \text{sign}(\xi) \frac{x + \xi^{-1}A}{\|x + \xi^{-1}A\|}.$$

For  $\xi > 0$ , let  $r' \geq \xi^{-1}$  be a constant, and let  $\mathcal{W} \subset \mathcal{S}_r^{\xi, A}$ . Then the linearity of the risk functional  $r$  and the homogeneity of  $\Lambda$  yield

$$\begin{aligned} \Lambda \{(r', \mathcal{W})\} &= \Lambda \left\{ y \in \mathcal{F}_+ : r \{ \xi^{-1}A(y^\xi - 1) \} + \xi^{-1} \geq r', \text{sign}(\xi) \frac{\xi^{-1}Ay^\xi}{\|\xi^{-1}Ay^\xi\|} \in \mathcal{W} \right\} \\ &= (\xi r')^{-1/\xi} \Lambda \left\{ y \in \mathcal{F}_+ : r(Ay^\xi) \geq 1, \frac{Ay^\xi}{\|Ay^\xi\|} \in \mathcal{W} \right\}, \\ &= (\xi r')^{-1/\xi} \Lambda \{ y \in \mathcal{F}_+ : r(Ay^\xi) \geq 1 \} \times \sigma_r(\mathcal{W}), \end{aligned}$$

where we define

$$\sigma_r(\mathcal{W}) = \frac{\Lambda \left\{ y \in \mathcal{F}_+ : r(Ay^\xi) \geq 1, \frac{Ay^\xi}{\|Ay^\xi\|} \in \mathcal{W} \right\}}{\Lambda \{ y \in \mathcal{F}_+ : r(Ay^\xi) \geq 1 \}}.$$

For  $\xi < 0$ , we proceed similarly with  $r' \leq -1$

$$\begin{aligned} \Lambda \{(r', \mathcal{W})\} &= \Lambda \left\{ y \in \mathcal{F}_+ : r \{ \xi^{-1}A(y^\xi - 1) \} + \xi^{-1} \leq r', \text{sign}(\xi) \frac{\xi^{-1}Ay^\xi}{\|\xi^{-1}Ay^\xi\|} \in \mathcal{W} \right\} \\ &= (\xi r')^{-1/\xi} \Lambda \left\{ y \in \mathcal{F}_+ : r(Ay^\xi) \geq 1, \frac{Ay^\xi}{\|Ay^\xi\|} \in \mathcal{W} \right\}, \end{aligned}$$

For  $\xi = 0$ , we use the change of variables  $\rho = r(x)$ ,  $w = \exp\{x - r(x)\}$ . As  $r$  is an evaluation function, i.e.,  $\exp\{r(\log x)\} = r(x)$ , so for any  $r' \geq 0$  we see that

$$\Lambda \{(r', \mathcal{W})\} = \Lambda [y \in \mathcal{F}_+ : r(y \exp A) \geq \exp r', \exp \{A \log y - r(A \log y)\} \in \mathcal{W}],$$

and the homogeneity of  $\Lambda$  yields

$$\begin{aligned}\Lambda\{(r', \mathcal{W})\} &= \exp(-r')\Lambda[y \in \mathcal{F}_+ : r(y \exp A) \geq 1, \exp\{A \log y - r(A \log y)\} \in \mathcal{W}] \\ &= \exp(-r')\Lambda\{y \in \mathcal{F}_+ : r(y \exp A) \geq 1\} \times \sigma_r(\mathcal{W}),\end{aligned}$$

with

$$\sigma_r^\xi(\mathcal{W}) = \frac{\Lambda[y \in \mathcal{F}_+ : r(y \exp A) \geq 1, \exp\{A \log y - r(A \log y)\} \in \mathcal{W}]}{\Lambda\{y \in \mathcal{F}_+ : r(y \exp A) \geq 1\}},$$

which proves the theorem.  $\square$

### B.3 Marginal properties of generalized $r$ -Pareto processes

For (14), we use the representation of generalized  $r$ -Pareto processes for non-linear functionals. Let  $s_0 \in S$ , and suppose that we found  $u' \geq 0$  such that

$$\left\{y \in \mathcal{F}^{\xi, a, b} : y(s_0) > \left\{1 + \xi \frac{u' - b(s_0)}{a(s_0)}\right\}^{1/\xi}\right\} \subset \left\{y \in \mathcal{F}_+ : r\left(A \frac{y^\xi - 1}{\xi}\right) \geq 0\right\}$$

Then,

$$\begin{aligned}\Pr\{P(s_0) > u'\} &= \Pr[P \in \{x \in \mathcal{F}^{\xi, a, b} : x(s_0) > u'\}] \\ &= \frac{\Lambda\left[y \in \mathcal{F}_+ : a(s_0) \frac{y^\xi(s_0) - 1}{\xi} + b(s_0) \geq u', r\left(A \frac{y^\xi - 1}{\xi}\right) \geq 0\right]}{\Lambda\left\{y \in \mathcal{F}_+ : r\left(A \frac{y^\xi - 1}{\xi}\right) \geq 0\right\}} \\ &= \left[1 + \xi \frac{(u' - u_0)}{a(s) + \xi\{u_0 - b(s_0)\}}\right]^{-1/\xi} \times \\ &\quad \frac{\Lambda\left\{y \in \mathcal{F}_+ : y^\xi(s_0) \geq 1 + \xi a(s_0)^{-1}\{u_0 - b(s_0)\}, r\left\{A \frac{y^\xi - 1}{\xi}\right\} \geq 0\right\}}{\Lambda\left\{y \in \mathcal{F}_+ : r\left(A \frac{y^\xi - 1}{\xi}\right) \geq 0\right\}},\end{aligned}$$

so for any  $r' \geq 0$

$$\begin{aligned}\Pr [P(s_0) > r' + u' | P(s_0) > u'] &= \frac{[1 + \xi a(s_0)^{-1} \{r' + u' - b(s_0)\}]^{-1/\xi}}{[1 + \xi a(s_0)^{-1} \{u' - b(s_0)\}]^{-1/\xi}} \\ &= \left[1 + \xi \frac{r'}{\sigma(u)}\right]^{-1/\xi},\end{aligned}$$

where  $\sigma(u') = a(s_0) + \xi \{u' - b(s_0)\}$ .

For a linear risk functional, the distribution of the  $r$ -intensity simplifies to

$$\begin{aligned}\Pr\{r(P) > r'\} &= \Pr [P \in \{x \in \mathcal{F}^{\xi, a, b} : r(x) \geq r'\}] \\ &= \frac{\Lambda \left[ y \in \mathcal{F}_+ : r \left( A \frac{y^\xi - 1}{\xi} \right) \geq \frac{r' - r(b)}{r(a)} \right]}{\Lambda \left\{ y \in \mathcal{F}_+ : r \left( A \frac{y^\xi - 1}{\xi} \right) \geq 0 \right\}} \\ &= \frac{\Lambda \left[ y \in \mathcal{F}_+ : r(Ay^\xi) \geq 1 + \xi \frac{r' - r(b)}{r(a)} \right]}{\Lambda \{ y \in \mathcal{F}_+ : r(Ay^\xi) \geq 1 \}} \\ &= \left[ 1 + \xi \frac{r' - r(b)}{r(a)} \right]^{-1/\xi},\end{aligned}$$

with  $r' \geq r(b)$ . □

## B.4 Derivation of (21)

For any  $\mathcal{A} \subset \{x \in \mathcal{F}^{\xi, a, b} : r \{(x - b)/r(a)\} \geq 0\}$ , we have

$$\begin{aligned}\Pr (P \in \mathcal{A}) &= \frac{\Lambda \left\{ y \in \mathcal{F}_+ : r \left( A \frac{y^\xi - 1}{\xi} \right) \geq 0, a \frac{y^\xi - 1}{\xi} + b \in \mathcal{A} \right\}}{\Lambda \left\{ y \in \mathcal{F}_+ : r \left( A \frac{y^\xi - 1}{\xi} \right) \geq 0 \right\}} \\ &= \frac{\Lambda \left[ \{1 + \xi a^{-1}(x - b)\}^{1/\xi} \in \mathcal{F}_+ : r \{(x - b)/r(a)\} \geq 0, x \in \mathcal{A} \right]}{\Lambda \left\{ y \in \mathcal{F}_+ : r \left( A \frac{y^\xi - 1}{\xi} \right) \geq 0 \right\}},\end{aligned}$$

and thus using a chain rule to compute partial derivatives with respect to the elements of the vector  $x$ , we get

$$\frac{\partial \Pr(P \in \cdot)}{\partial x} = \frac{\lambda \left\{ \left( 1 + \xi \frac{x-b}{a} \right)^{1/\xi} \right\}}{\Lambda \left\{ y \in \mathcal{F}_+ : r \left( A \frac{y^\xi - 1}{\xi} \right) \geq 0 \right\}} \prod_{l=1}^L a(s_l)^{-1} \left( 1 + \xi \frac{x-b(s_l)}{a(s_l)} \right)^{1/\xi-1},$$

which gives (21).

## C Windstorm Model Validation Plots

This Appendix gives the detailed plots of the logistic regression modelling the distribution of  $1\{r(x) \geq u\}$ , the probability of storm occurrence in Europe. The North Atlantic Oscillation (NAO) index and the first and third eigenvalues of the temperature anomaly, shown in Figures 13, 14 and 15, have a significant influence on the occurrence of winter storms at the 0.1% confidence level.

## D Diagnostic plots for the frequency of windstorms

Figure 16 shows the fitted daily probabilities of  $r$ -exceedances for the European windstorms.



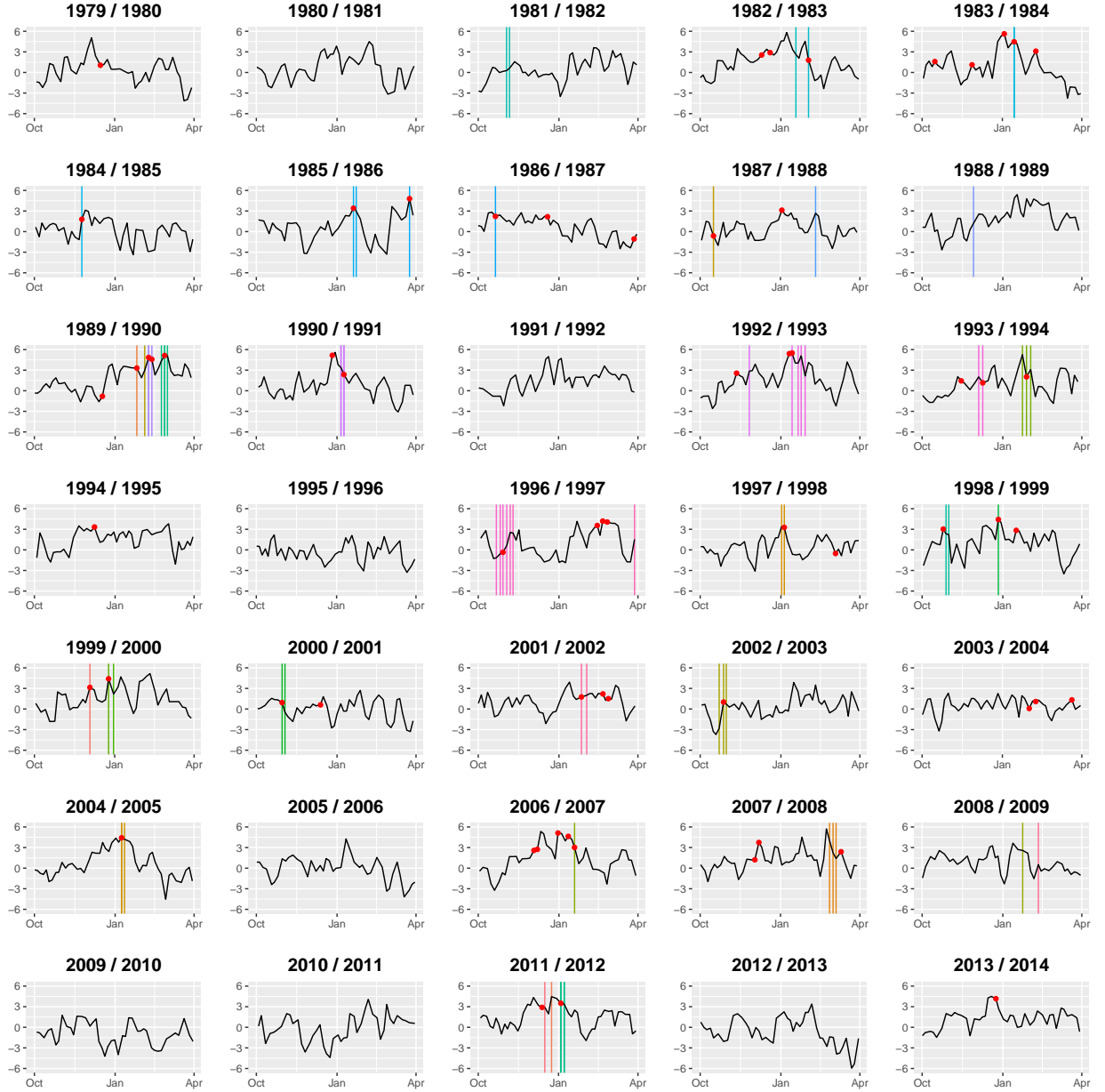


Figure 13: Three-hourly North Atlantic Oscillation (NAO) index computed on the ERA–Interim data set for each winter.  $r$ -exceedances above the 0.96 empirical quantile are represented by red dots and windstorms from XWS catalogue are represented by vertical lines coloured by dates.

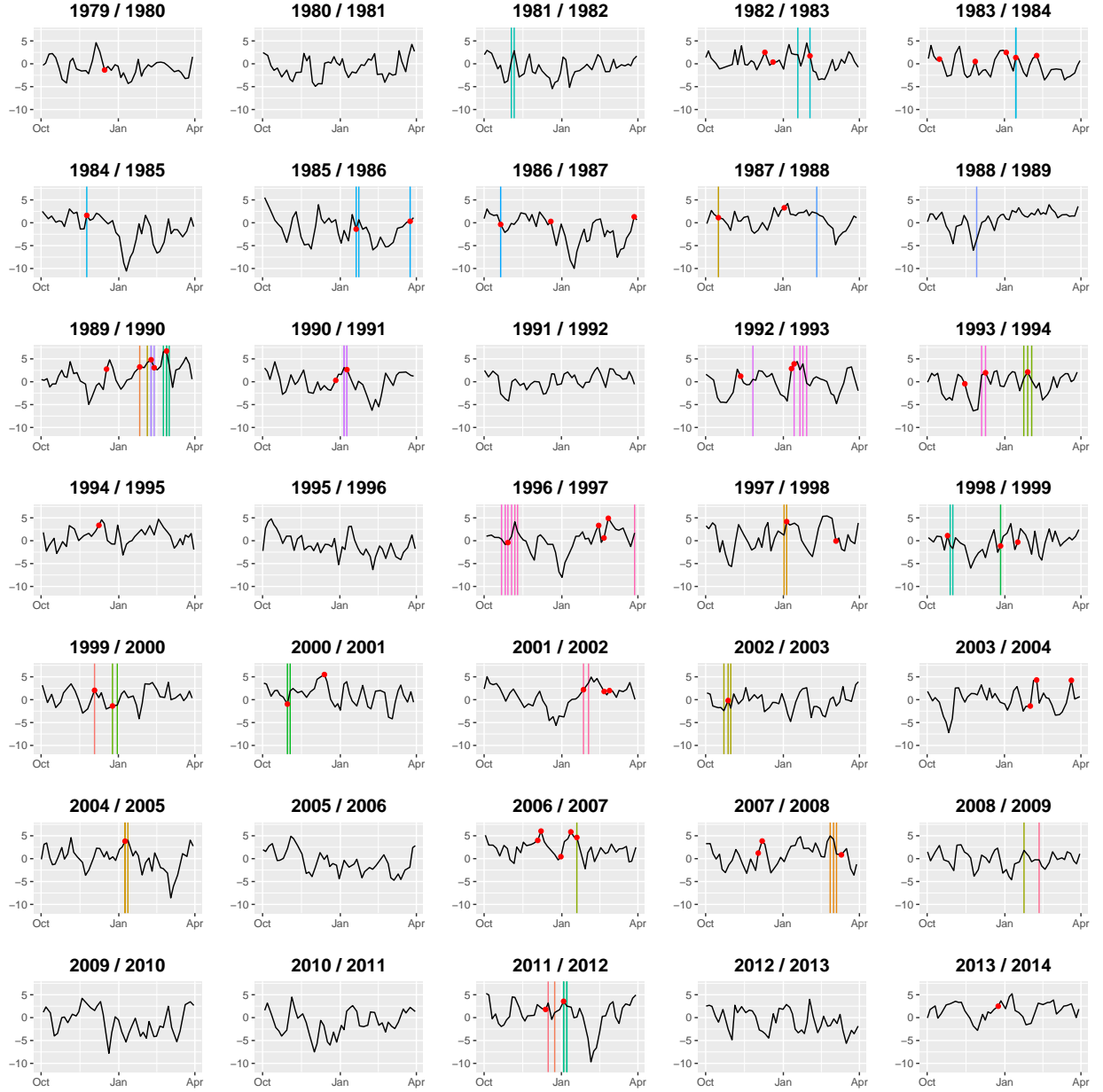


Figure 14: Three-hourly first eigenvalue of the spatial EOF decomposition of the temperature anomaly computed on the ERA–Interim data set for each winter.  $r$ -exceedances above the 0.96 empirical quantile are represented by red dots and windstorms from XWS catalogue are represented by vertical lines coloured by dates.

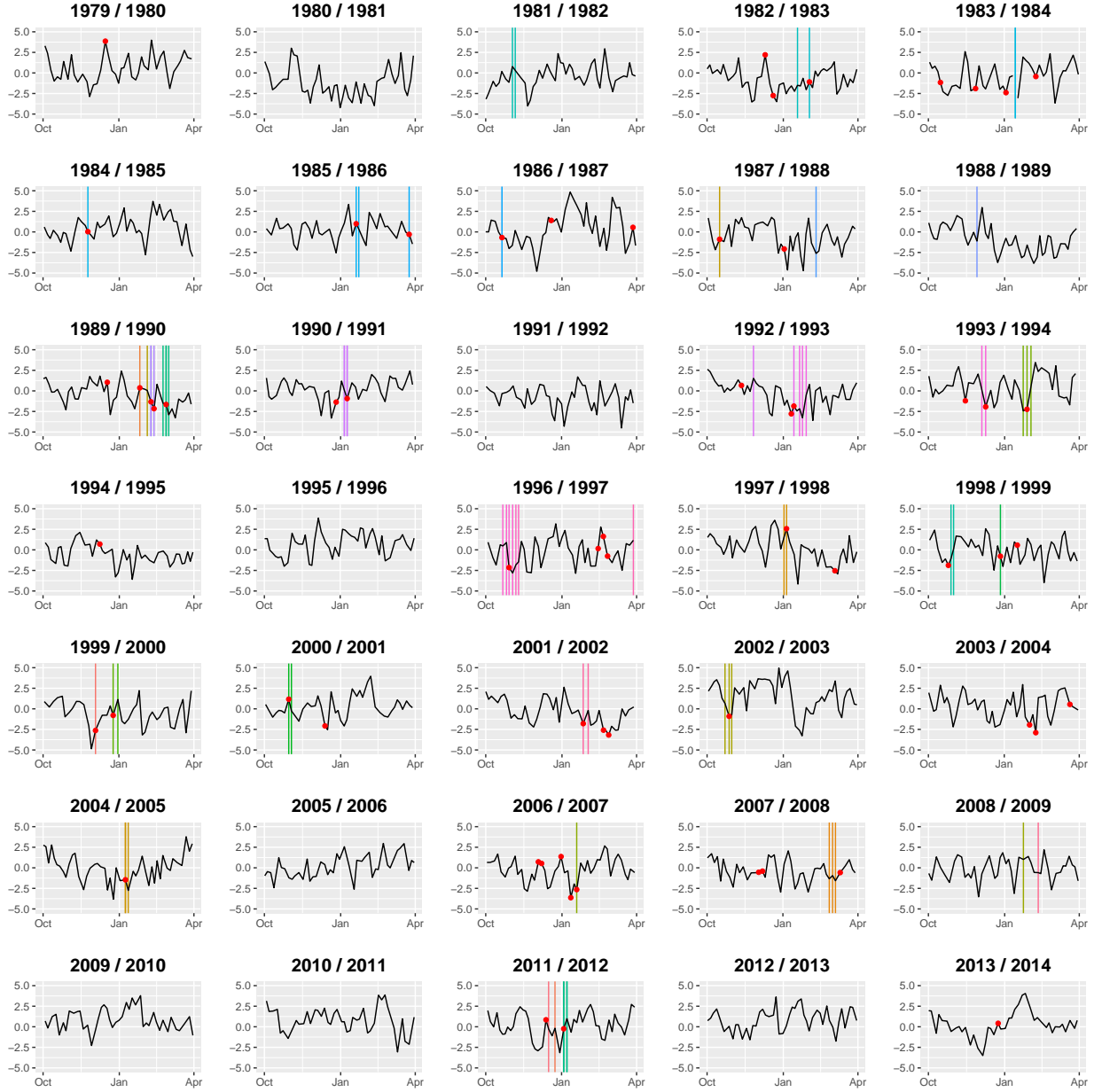


Figure 15: Three-hourly third eigenvalue of the spatial EOF decomposition of the temperature anomaly computed on the ERA–Interim data set for each winter.  $r$ -exceedances above the 0.96 empirical quantile are represented by red dots and windstorms from XWS catalogue are represented by vertical lines coloured by dates.

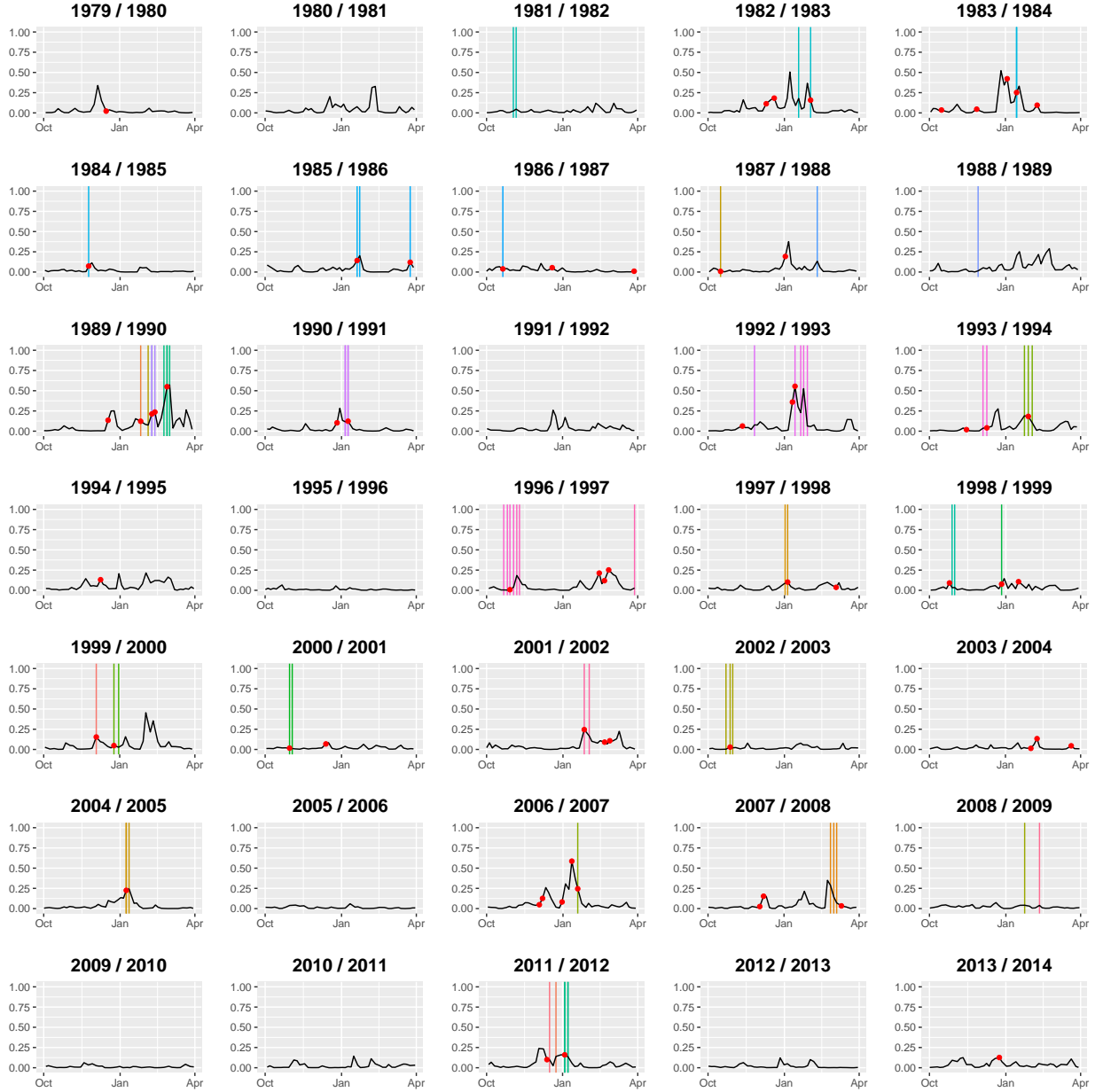


Figure 16: Three-hourly probability of  $r$ -exceedances using logistic regression model with the NAO index and the first and third temperature anomaly eigenvalues as covariates. Observed  $r$ -exceedances are represented by red points and the vertical lines coloured by dates correspond to the storms from the XWS catalogue.